The Loschmidt echo for local perturbations: escape-rate and oscillatory decay regimes

Arseni Goussev

Institut für Theoretische Physik, Universität Regensburg, 93040 Regensburg, Germany

School of Mathematics, University of Bristol, University Walk, Bristol BS8 1TW, United Kingdom‡

Daniel Waltner

Institut für Theoretische Physik, Universität Regensburg, 93040 Regensburg, Germany

Klaus Richter

Institut für Theoretische Physik, Universität Regensburg, 93040 Regensburg, Germany

Rodolfo A. Jalabert

Institut für Theoretische Physik, Universität Regensburg, 93040 Regensburg, Germany

Institut de Physique et Chimie des Matériaux de Strasbourg, UMR 7504 (CNRS-ULP), 23 rue du Loess, BP 43, 67034 Strasbourg Cedex 2, France§

Abstract. We address the sensitivity of quantum mechanical time evolution by considering the time decay of the Loschmidt echo (LE) (or fidelity) for local perturbations of the Hamiltonian. Within a semiclassical approach we derive analytical expressions for the LE decay for chaotic systems for the whole range from weak to strong local boundary perturbations and identify different decay regimes which complement those known for the case of (weak) global perturbations. For a strong perturbation, the LE decay is exponential, the escape-rate regime, with a rate independent of the perturbation strength, while the regime of intermediate perturbation strengths is characterized by distinct and pronounced oscillations of the LE, superimposed over the exponential decay. For weak perturbation a Fermi-golden-rule-type behavior is recovered. We further perform extensive quantum mechanical calculations of the LE based on numerical wave packet evolution which support our analytical semiclassical predictions and reveal precursors of the LE oscillations. Finally, we dicuss in some detail possible experimental realizations for observing the predicted novel decay oscillations.

‡ Present address

§ Present and permanent address

1. Introduction

One of the most prominent manifestations of chaos in classical physics is the hypersensitivity of the dynamics to perturbations in the initial conditions or Hamiltonian. That is, two trajectories of a chaotic system launched from two infinitesimally close phase-space points deviate exponentially from each other; so do the trajectories starting from the same point in phase space, but evolving under slightly different Hamiltonians. In a quantum system it is natural to consider $|\langle\phi_1|\phi_2\rangle|^2$ as a measure of "separation" of two quantum states $|\phi_1\rangle$ and $|\phi_2\rangle$. The unitarity of quantum propagators renders the overlap of any two states of the same system unchanged in the course of time. Thus, quantum systems are said to be stable with respect to perturbations of the initial state. However, a perturbation of the Hamiltonian can (and usually does) result in a nontrivial time dependence of the wave function overlap, suggesting a viable approach for describing instabilities and, therefore, for quantifying chaos in quantum systems.

Peres [1] proposed to consider the overlap

$$O(t) = \langle\phi_0|e^{i\tilde{H}t/\hbar}e^{-iHt/\hbar}|\phi_0\rangle \tag{1}$$

of the state $e^{-iHt/\hbar}|\phi_0\rangle$, resulting from an initial state $|\phi_0\rangle$ after evolution for a time t under the Hamiltonian H, with the state $e^{-i\tilde{H}t/\hbar}|\phi_0\rangle$ obtained from evolving the same initial state through t, but under a slightly different (perturbed) Hamiltonian $\tilde{H}$. He showed that the long-time behavior of

$$M(t) = |O(t)|^2 \tag{2}$$

depends on whether the underlying classical dynamics is regular or chaotic.

In the field of quantum computing $M(t)$ is an important concept, usually referred to as *fidelity* [2]. Moreover, $M(t)$ can be also interpreted as the squared overlap of the initial state $|\phi_0\rangle$ and the state obtained by first propagating $|\phi_0\rangle$ through time t under the Hamiltonian H, and then through time $-t$ under the perturbed Hamiltonian $\tilde{H}$ (or $-\tilde{H}$ from t to $2t$). This time-reversal interpretation constitutes a description of the echo experiments that have been performed by nuclear magnetic resonance since the fifties [3]. When the Hamiltonian H describes some complex (many-body or chaotic) dynamics $M(t)$ is referred to as *Loschmidt echo* (LE) [4], and this is the terminology we will adopt.

By construction, the LE equals unity at $t = 0$, and typically decays further in time. Most of the analytical studies so far addressed the quantity $\overline{M(t)}$ corresponding to the LE averaged either over an ensemble of initial states, or over an ensemble of different perturbed (and/or unperturbed) Hamiltonians. $\overline{M(t)}$ has been predicted to follow different decay regimes in various chaotic systems with several Hamiltonian perturbations [5, 6]. Depending on the nature and strength of the perturbation, $\tilde{H} - H$, one recognizes the *perturbative* Gaussian [7, 8, 9], the non-diagonal or *Fermi-golden-rule* (FGR) [5, 7, 8] and the diagonal or *Lyapunov* [5, 10] regimes. Here, 'diagonal' and 'non-diagonal' refer to the underlying pairing of interfering paths in a semiclassical approach, see Sec. 2. The perturbative, FGR and Lyapunov regimes, listed above in the order of the (properly defined) increasing perturbation strength, constitute the framework for classification of LE decay regimes [6, 11]. It is important to mention that the full variety of system- and perturbation-dependent decay regimes is rather rich, and extends far beyond the above list: double-Lyapunov [12], super-exponential [13] and power law [14] decay regimes serve as examples. We further note that analytical results for the time decay of the *unaveraged* LE, $M(t)$, are currently available only for very few chaotic systems [15].

The discovery [5] of the Lyapunov regime for the decay of the averaged LE in classically chaotic systems, $\overline{M(t)} \sim \exp(-\lambda t)$ with λ being the average Lyapunov exponent, provided a strong and appealing connection between classical and quantum chaos: it related a purely quantum measure of instability, such as the LE, to a quantity characterizing the corresponding classical instability, i.e. the Lyapunov exponent. This result awoke the interest on the LE in the quantum chaos community. The Lyapunov regime has been numerically observed in several two-dimensional chaotic systems, i.e. in the Lorentz gas [10, 16], the Bunimovich stadium [17], the smooth stadium billiard [18], a Josephson flux qubit device [19], as well as in one-dimensional time-dependent Hamiltonian systems [7].

The theory of the Lyapunov decay of the LE mainly relies on the following two assumptions: (i) the validity of the structural stability arguments (supported by the shadowing theorem [20]), and (ii) the global nature of the Hamiltonian perturbation. The first assumption guaranties a unique one-to-one mapping of trajectories of the unperturbed system to those of the perturbed system. This mapping allows for efficient pairing of the trajectories of the unperturbed and perturbed system in the diagonal approximation [21]. The second assumption implies that the Hamiltonian perturbation affects every trajectory of the system, and, therefore, all trajectories are responsible for the decay of the LE. However, this is by no means the most general situation when we consider possible experimental realizations of the LE.

In the present work we extend the semiclassical theory of the LE by lifting the second of the two above-mentioned assumptions, i.e. *we allow for a local perturbation in coordinate space.* In this context the LE decay was previously addressed in the case of a *strong* local perturbation [22], i.e. for a billiard exposed to a local boundary deformation much larger than the de Broglie wavelength. Analytical and numerical calculations yielded a novel LE decay regime, for which $M(t) \sim \exp(-2\gamma t)$ with γ being the probability (per unit time) of the corresponding classical particle to encounter the boundary deformation. γ can also be viewed as a classical *escape rate* from a related open billiard obtained from the original (closed) one by removing the deformation-affected boundary segment. In this work we explore all strengths of a local perturbation and uncover a sequence of decay regimes of the LE that completes the previous picture. In particular, we predict a novel *oscillatory* decay regime for intermediate perturbation strengths: we find that the LE oscillates wildly as a function of time around an exponentially decaying envelope.

The paper is organized as follows: In Section 2 we develop a comprehensive semiclassical approach of the LE decay due to local Hamiltonian perturbations of increasing strength. We perform a systematic analysis of the different decay regimes, establish their relation to the previously known decay regimes in the case of a global perturbation, and identify an oscillatory behavior in the LE decay. In Section 3 we validate our semiclassical theory by numerical calculations and discuss the onset of the decay oscillations. In Sec. 4 we outline possible experimental realizations and focus on the possibility of introducing a local perturbation in a microwave-cavity and cold-atom LE setup in order to obtain the signature of the decay oscillations. We provide concluding remarks in Sec. 5 and point to the similarities and differences with respect to other non-monotonous LE decays previously reported in the literature. Technical aspects of the calculations are relegated to the appendices.

2. Semiclassical approach

2.1. Wave-function evolution

We address the time evolution of the wave function that describes a quantum particle moving inside a classically chaotic two-dimensional billiard (corresponding to a Hamiltonian H). We assume that initially (at time $t = 0$) the particle is in a coherent state

$$\phi_0(\mathbf{r}) = \frac{1}{\sqrt{\pi}\sigma} \, \exp\left[\frac{i}{\hbar}\mathbf{p}_0 \cdot (\mathbf{r} - \mathbf{r}_0) - \frac{(\mathbf{r} - \mathbf{r}_0)^2}{2\sigma^2}\right] . \tag{3}$$

Here σ quantifies the extension of the Gaussian wave packet, while $\mathbf{r}_0$ and $\mathbf{p}_0$ are the initial mean values of the position and momentum operators, respectively. We further define the de Broglie wavelength of the particle as $\lambda_{\mathrm{B}} = \hbar/p_0$. Notice that in our definition of λ_{B} there is a factor of 2π with respect to the standard convention used for the de Broglie wavelength.

In our description of the time evolution of the wave function we rely on the semiclassical approximation [23] of the wave function at a time t,

$$\phi_t(\mathbf{r}) = \int d\mathbf{r}' \sum_{\hat{s}(\mathbf{r},\mathbf{r}',t)} \mathcal{K}_{\hat{s}}(\mathbf{r},\mathbf{r}',t)\phi_0(\mathbf{r}') \, . \tag{4}$$

Here

$$\mathcal{K}_{\hat{s}}(\mathbf{r},\mathbf{r}',t) = \frac{\sqrt{D_{\hat{s}}}}{2\pi i\hbar} \, \exp\left[\frac{i}{\hbar}S_{\hat{s}}(\mathbf{r},\mathbf{r}',t) - i\frac{\pi\nu_{\hat{s}}}{2}\right] \tag{5}$$

is the contribution to the Van Vleck propagator associated with the classical trajectory $\hat{s}(\mathbf{r},\mathbf{r}',t)$ leading from point $\mathbf{r}'$ to point $\mathbf{r}$ in time t. $S_{\hat{s}}(\mathbf{r},\mathbf{r}',t)$ denotes the classical action integral (or the Hamilton principal function) along the path $\hat{s}$. In a hard-wall billiard $S_{\hat{s}}(\mathbf{r},\mathbf{r}',t) = (m/2t)L^2_{\hat{s}}(\mathbf{r},\mathbf{r}')$, where $L_{\hat{s}}(\mathbf{r},\mathbf{r}')$ is the length of the trajectory $\hat{s}$, and m is the mass of the particle. In Eq. (5), $D_{\hat{s}} = |\det(-\partial^2 S_{\hat{s}}/\partial\mathbf{r}\partial\mathbf{r}')|$, and the Maslov index $\nu_{\hat{s}}$ equals the number of caustics along the trajectory $\hat{s}$ plus twice the number of particle-wall collisions (for the case of Dirichlet boundary conditions).

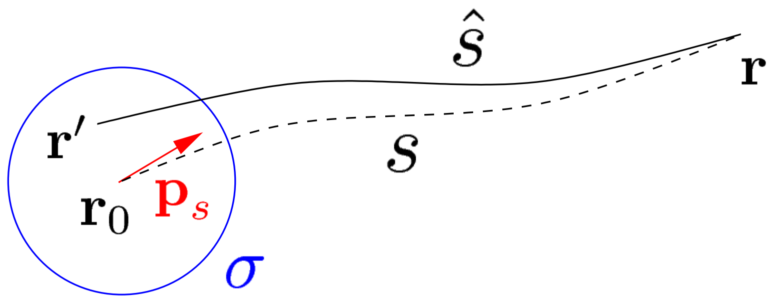

Figure 1. Sketch of a typical trajectory $\hat{s}$ (full line), connecting a point $\mathbf{r}'$ (within the circular extension of radius σ of the initial wave packet) to the point $\mathbf{r}$, where the evolved wave function is evaluated, together with the central trajectory s (dashed line) that reaches the same final point, but starts at the center $\mathbf{r}_0$ of the wave packet (with momentum $\mathbf{p}_s$). The linearization of Eq. (6), together with the conditions discussed in the text, allow to represent all the trajectories $\hat{s}$ contributing to Eq. (4) by the single reference trajectory s.

Since we assume that the initial wave packet is localized around $\mathbf{r}_0$ within σ, only trajectories starting at points $\mathbf{r}'$ close to $\mathbf{r}_0$ are relevant for our semiclassical description. Thus we can expand the action integral $S_{\hat{s}}(\mathbf{r}, \mathbf{r}', t)$ in a power series in $(\mathbf{r}' - \mathbf{r}_0)$. In Appendix Appendix A we show that the power series can be terminated at the linear term,

$$S_{\hat{s}}(\mathbf{r}, \mathbf{r}', t) \approx S_s(\mathbf{r}, \mathbf{r}_0, t) - \mathbf{p}_s \cdot (\mathbf{r}' - \mathbf{r}_0) \ , \tag{6}$$

if the wave packet is narrow enough, so that the condition

$$\sigma \ll \sqrt{\frac{l_{\mathrm{L}}}{1/\lambda_{\mathrm{B}} + 1/\sigma}} \tag{7}$$

is satisfied, where $l_{\mathrm{L}} = p_0/m\lambda$ is the Lyapunov length. In Eq. (6), $s(\mathbf{r}, \mathbf{r}_0, t)$ is the *central* reference trajectory into which $\hat{s}(\mathbf{r}, \mathbf{r}', t)$ gets uniformly deformed as $\mathbf{r}' \to \mathbf{r}_0$, and $\mathbf{p}_s = -\partial S_s(\mathbf{r}, \mathbf{r}_0, t)/\partial \mathbf{r}_0$ denotes the initial momentum of the trajectory s (see Fig. 1).

Substituting Eq. (6) into Eq. (5), and performing the integration in Eq. (4) we obtain

$$\phi_t(\mathbf{r}) = 2\pi\hbar \sum_{s(\mathbf{r}, \mathbf{r}_0, t)} \mathcal{K}_s(\mathbf{r}, \mathbf{r}_0, t) \ \Phi_0(\mathbf{p}_s) \ , \tag{8}$$

with

$$\begin{aligned} \Phi_0(\mathbf{p}) &\equiv \int \frac{d\mathbf{r}}{2\pi\hbar} \exp\left[-\frac{i}{\hbar}\mathbf{p} \cdot (\mathbf{r} - \mathbf{r}_0)\right] \phi_0(\mathbf{r}) \\ &= \frac{\sigma}{\sqrt{\pi}\hbar} \exp\left[-\frac{\sigma^2}{2\hbar^2}(\mathbf{p} - \mathbf{p}_0)^2\right] \end{aligned} \tag{9}$$

the momentum representation of the initial wave packet.

We now consider a related billiard, corresponding to the perturbed Hamiltonian $\tilde{H}$, that differs from the original (unperturbed) billiard by a deformation of the boundary segment $\mathcal{B}_1$ of width w (see Fig. 2). The perturbation is thus local, and will be

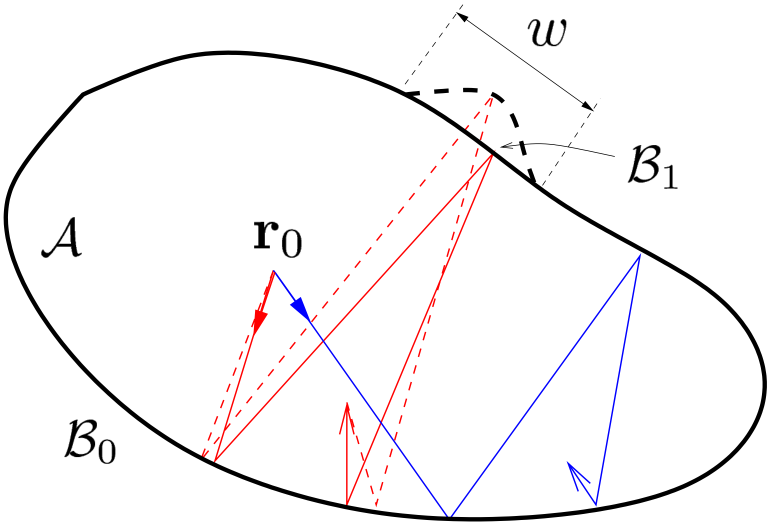

Figure 2. Sketch of our model system of a particle moving inside a chaotic billiard of area $\mathcal{A}$. The perturbation consists of a deformation localized in a region $\mathcal{B}_1$ (of width w) of the billiard boundary. The complementary set $\mathcal{B}_0$ of the boundary is unaffected by the perturbation. The two trajectories s (red solid line) and $\hat{s}$ (red dashed line) starting from $\mathbf{r}_0$ with different momenta correspond, respectively, to the unperturbed and perturbed Hamiltonian. The diagonal approximation entering Eq. (12) identifies both of them and assigns an action difference given by Eq. (15). The starting momentum of the solid red trajectory belongs to the set $\mathcal{P}_1$. The third trajectory (blue solid line) hits the boundary only at $\mathcal{B}_0$ and therefore is the same for both the unperturbed and perturbed systems. Hence the action difference of the corresponding trajectory pair is zero. The starting momentum of the blue trajectory belongs to the set $\mathcal{P}_0$.

characterized by its extent (depending on the ratio between w and the cavity perimeter P) and its strenght (that will be quantified in the sequel). In view of Eq. (8), the wave function describing the evolution of the particle (starting from the same initial state ϕ_0) can be written as

$$\tilde{\phi}_t(\mathbf{r}) = 2\pi\hbar \sum_{\tilde{s}(\mathbf{r},\mathbf{r}_0,t)} \mathcal{K}_{\tilde{s}}(\mathbf{r},\mathbf{r}_0,t)\Phi_0(\mathbf{p}_{\tilde{s}})\,. \tag{10}$$

The sum now runs over all possible trajectories $\tilde{s}(\mathbf{r},\mathbf{r}_0,t)$ of a classical particle that travels from $\mathbf{r}_0$ to $\mathbf{r}$ in time t while bouncing off the boundary of the perturbed billiard.

2.2. Wave-function overlap for local perturbations

According to Eqs. (8)-(10) and the definition (1) of the LE amplitude, we have

$$\begin{aligned} O(t) &= \int_{\mathcal{A}} d\mathbf{r}\ \tilde{\phi}_t^*(\mathbf{r})\phi_t(\mathbf{r}) \qquad (11)\\ &= \int_{\mathcal{A}} d\mathbf{r} \sum_{\tilde{s}}\sum_{s} \sqrt{D_{\tilde{s}}D_s} \\ &\quad \times \exp\left[\frac{i}{\hbar}(S_s - S_{\tilde{s}}) - i\frac{\pi(\nu_s-\nu_{\tilde{s}})}{2}\right] \Phi_0^*(\mathbf{p}_{\tilde{s}})\Phi_0(\mathbf{p}_s)\,, \end{aligned}$$

where $\mathcal{A}$ stands for the billiard area. The shadowing theorem [20] allows us to employ the diagonal approximation ($s \simeq \tilde{s}$) in the case of a classically small perturbation, thus reducing Eq. (12) to

$$O(t) = \int_{\mathcal{A}} d\mathbf{r} \sum_{s(\mathbf{r},\mathbf{r}_0,t)} D_s \; \exp\left[\frac{i}{\hbar}\Delta S_s(\mathbf{r},\mathbf{r}_0,t)\right] W_0(\mathbf{p}_s)\,, \tag{12}$$

where

$$W_0(\mathbf{p}) \equiv |\Phi_0(\mathbf{p})|^2 = \frac{\sigma^2}{\pi\hbar^2}\; \exp\left[-\frac{\sigma^2}{\hbar^2}(\mathbf{p}-\mathbf{p}_0)^2\right] \tag{13}$$

is the probability distribution of the particle momentum. In billiards the action difference between the two trajectories traveling between the same initial and final points in the same time t can be written, in terms of their length difference ΔL_s, as

$$\begin{aligned} \Delta S_s(\mathbf{r},\mathbf{r}_0,t) &\equiv S_s - S_{\tilde{s}} \\ &= \frac{p_s^2}{2m}t - \frac{p_{\tilde{s}}^2}{2m}t \approx p_s\frac{p_s - p_{\tilde{s}}}{m}t = p_s\;\Delta L_s(\mathbf{r},\mathbf{r}_0,t)\,. \end{aligned} \tag{14}$$

Using the Jacobian property of the Van Vleck determinant D_s, we can replace the integral over final coordinates in Eq. (12) by an integral over the initial momenta and obtain

$$O(t) = \int d\mathbf{p}\; \exp\left[\frac{i}{\hbar}\; p\;\Delta L(\mathbf{r}_0,\mathbf{p}t)\right] W_0(\mathbf{p})\,. \tag{15}$$

The dependence of ΔL on the product $\mathbf{p}t$ stems from the fact that in billiards, changing the magnitude of the momentum only modifies the traveling time, but does not affect the path.

We now introduce a momentum set $\mathcal{P}_0(\mathbf{r}_0,t)$ such that for any $\mathbf{p} \in \mathcal{P}_0$ the classical trajectory, starting from the phase-space point $(\mathbf{r}_0,\mathbf{p})$, arrives at a coordinate-space point $\mathbf{r} \in \mathcal{A}$ after time t while undergoing collisions only with the part of the boundary unaffected by the deformation ($\mathcal{B}_0$ in Fig. 2). The complementary set, corresponding to trajectories that hit $\mathcal{B}_1$ at least once, is denoted by $\mathcal{P}_1$. For the set $\mathcal{P}_0$ we have $\Delta L = 0$, and therefore

$$O(t) = O_0(t) + O_1(t)\,, \tag{16}$$

with

$$O_0(t) = \int_{\mathcal{P}_0} d\mathbf{p}\; W_0(\mathbf{p})\,, \tag{17}$$

$$O_1(t) = \int_{\mathcal{P}_1} d\mathbf{p}\; W_0(\mathbf{p})\; e^{ip\Delta L(\mathbf{r}_0,\mathbf{p}t)/\hbar}\,. \tag{18}$$

Since we are studying billiards, the integrations over momenta can be simplified by working in polar coordinates (p,θ) and considering the set $\Theta_0(\mathbf{r}_0,pt)$ of angles θ such that $\mathbf{p} \equiv (p,\theta) \in \mathcal{P}_0(\mathbf{r}_0,t)$ iff $\theta \in \Theta_0$. The complementary set is denoted by Θ_1. For a classically chaotic dynamics the set Θ_0 shrinks with increasing time t, and Θ_0 becomes the fractal set defining the repeller of the corresponding open (scattering) problem in the limit $t \to \infty$. Eqs. (17) and (18) can, respectively, be written as

$$O_0(t) = \int_0^\infty dpp \int_{\Theta_0} d\theta \; W_0(\mathbf{p}) \,, \tag{19}$$

$$O_1(t) = \int_0^\infty dpp \int_{\Theta_1} d\theta \; W_0(\mathbf{p}) \; e^{ip\Delta L(\mathbf{r}_0, pt, \theta)/\hbar} \,. \tag{20}$$

For long times t, where many trajectories contribute to the semiclassical expansions, the angular integrals over Θ_0 and Θ_1 can be replaced by integrals over all angles, weighted with the measures $\exp(-pt/ml_\mathrm{d})$ and $(1-\exp(-pt/ml_\mathrm{d}))$ of the corresponding set. Here l_d is the average dwell length of paths in the related open chaotic billiard obtained from the original (closed) one by removing the boundary region $\mathcal{B}_1$. The measure of Θ_0 follows from the probability per unit time that a particle encounters the boundary deformation. This corresponds to the classical escape rate of the open cavity that for particles with momentum p_0 is given by

$$\gamma = \frac{p_0}{ml_\mathrm{d}} \,. \tag{21}$$

For a chaotic cavity with an opening w much smaller than its perimeter P we can approximate [24] $l_\mathrm{d} \approx \pi\mathcal{A}/w$, and therefore

$$\gamma \approx \frac{p_0}{m} \, \frac{w}{\pi\mathcal{A}} \,. \tag{22}$$

In our case the escape rate γ yields a measure of the perturbation extent. The classical escape rate of an open cavity controls the fluctuations of the transmission coefficients, and therefore approximations such as (22) have been thoroughly examined in the context of quantum transport [25].

According to the previous discussion we can approximate $O_0(t)$ and $O_1(t)$, respectively, by the averages

$$\bar{O}_0(t) = \int_0^\infty dp \; p \, e^{-pt/ml_\mathrm{d}} \int_0^{2\pi} d\theta \; W_0(\mathbf{p}) \,, \tag{23}$$

$$\bar{O}_1(t) = \int_0^\infty dp \; p \left\langle e^{ip\Delta L(\mathbf{r}_0, pt, \theta)/\hbar} \right\rangle \left(1 - e^{-pt/ml_\mathrm{d}}\right) \int_0^{2\pi} d\theta \; W_0(\mathbf{p}) \,. \tag{24}$$

The mean value $\langle \ldots \rangle$ should be taken over the set $\Theta_1(\mathbf{r}_0, pt)$. The chaotic nature of the dynamics will enable us to treat the averages over Θ_1 in a statistical way. In view of Eq. (13), the θ-integral in Eqs. (23) and (24) yields

$$\int_0^{2\pi} d\theta W_0(\mathbf{p}) = \frac{2\sigma^2}{\hbar^2} \exp\left[-\frac{\sigma^2}{\hbar^2}\left(p^2 + p_0^2\right)\right] I_0\left(\frac{2\sigma^2}{\hbar^2} p_0 p\right) , \tag{25}$$

where I_0 denotes the modified Bessel function.

As usually assumed in the Loschmidt echo studies, we restrict our analysis to "semiclassical" initial wave packets $\phi_0(\mathbf{r})$ with sizes much larger than the de Broglie wave length,

$$\lambda_\mathrm{B} \ll \sigma \,. \tag{26}$$

This assumption, together with condition (7), defines the interval for the dispersion σ, where the semiclassical approach is reliable, and hence yields restrictions to the parameters of the billiard. Employing condition (26) enables us to use the asymptotic form $I_0(x) \approx e^x/\sqrt{2\pi x}$, valid for large x, in Eq. (25). Thus, the probability distribution function for the magnitude of the initial momentum is given by

$$p \int_0^{2\pi} d\theta W_0(\mathbf{p}) \approx \frac{\sigma}{\hbar}\sqrt{\frac{p}{\pi p_0}} \ \exp\left[-\frac{\sigma^2}{\hbar^2}(p-p_0)^2\right]. \tag{27}$$

We note that Eq. (27) provides a good approximation to the exact distribution function already for $\sigma \gtrsim 2\lambda_{\mathrm{B}}$. Under this assumption the p-integrals in Eqs. (23) and (24) are dominated by the contributions around p_0, and we can write

$$\bar{O}_0(t) \approx e^{-\gamma t} \quad \text{and} \quad \bar{O}_1(t) \approx \left(1 - e^{-\gamma t}\right) \left\langle e^{ip_0 \Delta L(\mathbf{r}_0, p_0 t, \theta)/\hbar} \right\rangle. \tag{28}$$

Since in Eq. (28) all classical quantities are evaluated for an initial momentum with magnitude p_0, the mean value $\langle \dots \rangle$ should be taken over the set $\Theta_1(\mathbf{r}_0, p_0 t)$. However, for long times and a chaotic dynamics we do not expect these mean values to depend on $\mathbf{r}_0$. In the next section we will further invoke the chaotic nature of the underlying classical dynamics in order to estimate the mean values and therefore the LE average amplitude.

2.3. Averages over trajectory distributions

For classically small perturbations the action, respectively, length difference (Eq. (15)) between a trajectory s (solid red segment in Fig. 2) and its perturbed partner $\tilde{s}$ (dashed segment) is given only by the contributions accumulated along the N encounters with $\mathcal{B}_1$. Differences in length arising from the free flights between collisions with the boundary $(\mathcal{B}_0 + \mathcal{B}_1)$ are of higher order in the perturbation strength and will not be considered. We can then write

$$\Delta L = \sum_{j=1}^{N} u(\vartheta_j, \xi_j)\,, \tag{29}$$

where the deformation function $u(\vartheta_j, \xi_j)$ is the length difference accumulated in the j-th collision with $\mathcal{B}_1$, depending on the impinging angle $\vartheta_j \in (-\pi/2, \pi/2)$ and on the coordinate $\xi_j \in (0, w)$ of the hitting point. The number N of collisions with $\mathcal{B}_1$ is a fraction of the total number of collisions $p_0 t/m l_{\mathrm{f}}$. The mean bouncing length l_{f} can be approximated by $\pi\mathcal{A}/P$, and we suppose $l_{\mathrm{d}} \gg l_{\mathrm{f}}$ since $P \gg w$. We note that for small perturbations ΔL depends on p only through N.

Given the chaotic nature of the classical dynamics and the fact that the collisions with $\mathcal{B}_1$ are typically separated by many collisions with $\mathcal{B}_0$ we assume ϑ_j, ξ_j, N and ΔL to be random variables. Treating the length of the free flights as uncorrelated Gaussian variables yields the probability distribution

$$P_N(N, t) \approx \frac{1}{\sqrt{2\pi\gamma t}} \exp\left[-\frac{(N-\gamma t)^2}{2\gamma t}\right] \tag{30}$$

for the number of collisions with $\mathcal{B}_1$. This expression is valid if $N \gg 1$ (i.e. for $t \gg \gamma^{-1}$) and in the case where the total number of bounces is much larger than N.

The first and the second moments of the above distribution are given, respectively, by

$$\langle N\rangle = \gamma t \qquad \text{and} \qquad \langle N^2\rangle - \langle N\rangle^2 = \gamma t\,. \tag{31}$$

Assuming a perfect randomization of the trajectories within the billiard the probability distribution functions for $\{\vartheta_j\}$ and $\{\xi_j\}$ are, respectively,

$$P_\vartheta(\vartheta) = \frac{\cos\vartheta}{2} \qquad \text{and} \qquad P_\xi(\xi) = \frac{1}{w}\,. \tag{32}$$

Treating the random variables as uncorrelated, we find for the first two moments of ΔL

$$\langle \Delta L\rangle = \langle N\rangle\langle u\rangle = \langle u\rangle\gamma t \tag{33}$$

and

$$\begin{aligned}\left\langle(\Delta L)^2\right\rangle &= \left\langle \sum_{j=1}^{N}\sum_{k=1}^{N} u(\vartheta_j,\xi_j)u(\vartheta_k,\xi_k)\right\rangle \\ &= \langle N\rangle\langle u^2\rangle + \langle(N^2-N)\rangle\langle u\rangle^2.\end{aligned} \tag{34}$$

Using Eq. (31) we then obtain for the variance of ΔL

$$\begin{aligned}\left\langle(\Delta L)^2\right\rangle - \langle\Delta L\rangle^2 &= \langle N\rangle\left(\langle u^2\rangle - \langle u\rangle^2\right) + \left(\langle N^2\rangle - \langle N\rangle^2\right)\langle u\rangle^2 \\ &= \langle u^2\rangle\gamma t\,.\end{aligned} \tag{35}$$

The deformation function has the moments

$$\langle u^n\rangle = \int_{-\pi/2}^{\pi/2} d\vartheta P_\vartheta(\vartheta)\int_0^w d\xi P_\xi(\xi)u^n(\vartheta,\xi) \tag{36}$$

that for $n=1$ and 2 carry the dimensions of length and squared length, respectively. Once we specify the shape of the perturbation, the moments of Eq. (36) are readily calculated from the probability distributions of Eq. (32). For instance, for a piston-like deformation (see Appendix Appendix B) ,

$$u(\vartheta,\xi) = 2h\cos\vartheta\,, \tag{37}$$

and the moments read $\langle u\rangle = h\pi/2$ and $\langle u^2\rangle = 8h^2/3$.

However, at this stage we will keep our discussion general and do not specify the details of the local perturbation. It is convenient to scale the first and second moment of u by the de Broglie wave length by introducing the dimensionless quantities

$$\Omega \equiv \frac{\langle u\rangle}{\lambda_{\rm B}} \qquad \text{and} \qquad \chi \equiv \frac{\langle u^2\rangle}{2{\lambda_{\rm B}}^2}\,. \tag{38}$$

In the large-N limit the Central Limit Theorem dictates that ΔL behaves as a Gaussian random variable, and therefore

$$\left\langle e^{ip_0\Delta L/\hbar}\right\rangle \approx \exp\left[i\frac{\langle\Delta L\rangle}{\lambda_{\rm B}} - \frac{\langle(\Delta L)^2\rangle - \langle\Delta L\rangle^2}{2{\lambda_{\rm B}}^2}\right] = \exp\left(i\Omega\gamma t - \chi\gamma t\right). \tag{39}$$

Substituting (39) into Eq. (28) yields the average LE amplitude. The latter is usually not an observable quantity, however it will be helpful towards our semiclassical calculation of the LE. The condition of a classically small perturbation that we have adopted throughout our work, implies that $\langle u \rangle \ll w \ll P$. Quantum mechanically the perturbation is characterized by a mean value Ω of the deformation (in units of λ_{B}) and a deformation strength given by χ. In most cases of LE studied so far the mean value of the perturbation vanishes. In our case we will have $\Omega \neq 0$ for $\langle u \rangle \neq 0$. That is, a characteristic phase is accumulated upon each encounter of the classical trajectories with $\mathcal{B}_1$. For instance, for piston-like deformations $\Omega = \pi/2(h/\lambda_{\mathrm{B}}) > 0$ since the deformation is always outwards. The non-zero value of Ω will translate into an oscillatory behavior superimposed to the decay of $\bar{O}_1(t)$. For $\chi \ll 1$ we will be in the quantum perturbative regime [7, 8, 9], which will not be considered in this work. Increasing the deformation strength χ we anticipate a richer variety of regimes than for the case of LE under global perturbations [5, 6] since the perturbation extent, quantified by γ, is another relevant parameter.

2.4. Loschmidt echo for local perturbations

According to Eqs. (2) and (12) the semiclassical expansion for the LE contains terms involving four trajectories. The diagonal approximation, leading to Eq. (12) for the LE amplitude, reduces the LE to a sum over pairs of trajectories. Consequently, the semiclassical form of the LE must take into account the different possibilities for each trajectory of the pair to hit (or not) the region of the boundary where the perturbation acts. We can therefore decompose the LE as

$$M(t) = M^{\mathrm{nd}}(t) + M^{\mathrm{d}}(t)\,, \tag{40}$$

where we have introduced the non-diagonal and diagonal contributions according to

$$\begin{aligned} M^{\mathrm{nd}}(t) = & \int_{\mathcal{P}_0} d\mathbf{p} W_0(\mathbf{p}) \int_{\mathcal{P}_0} d\mathbf{p}' W_0(\mathbf{p}') \\ & + 2\Re \left\{ \int_{\mathcal{P}_0} d\mathbf{p} W_0(\mathbf{p}) \int_{\mathcal{P}_1} d\mathbf{p}' W_0(\mathbf{p}') e^{ip'\Delta L(\mathbf{r}_0,\mathbf{p}'t)/\hbar} \right\} \\ & + \int_{\mathcal{P}_1} d\mathbf{p} W_0(\mathbf{p}) e^{-ip\Delta L(\mathbf{r}_0,\mathbf{p}t)/\hbar} \int_{\mathcal{P}_1 \setminus \varepsilon_{\mathbf{p}}} d\mathbf{p}' W_0(\mathbf{p}') e^{ip'\Delta L(\mathbf{r}_0,\mathbf{p}'t)/\hbar} \end{aligned} \tag{41}$$

and

$$\begin{aligned} M^{\mathrm{d}}(t) = & \int_{\mathcal{P}_1} d\mathbf{p} W_0(\mathbf{p}) \int_{\varepsilon_{\mathbf{p}}} d\mathbf{p}' W_0(\mathbf{p}') \\ & \times \exp\left\{ \frac{i}{\hbar} \left[p'\Delta L(\mathbf{r}_0,\mathbf{p}'t) - p\Delta L(\mathbf{r}_0,\mathbf{p}t) \right] \right\}. \end{aligned} \tag{42}$$

The set $\varepsilon_{\mathbf{p}}$ of momenta $\mathbf{p}'$ is defined such that two trajectories starting from the phase space points $(\mathbf{r}_0, \mathbf{p})$ and $(\mathbf{r}_0, \mathbf{p}')$, stay "close" to each other in phase space during time t, and thus are "correlated" with respect to the perturbation. We give a quantitative definition to $\varepsilon_{\mathbf{p}}$ below. Following the standard notation introduced in Ref. [5], we call diagonal term the one resulting from the identification of pairs of trajectories where the effect of the perturbation is correlated, that is, when $\mathbf{p}' \in \varepsilon_{\mathbf{p}}$. In the non-diagonal term we consider the pairs of trajectories uncorrelated with respect to the perturbation, including the case where one or both orbits are unperturbed. As noted at the beginning of this section, each of the trajectories of the above pair already incorporates a diagonal approximation between a perturbed and an unperturbed trajectories with the same extreme points.

2.5. Non-diagonal contribution to the Loschmidt echo

Calculating the LE as an average over trajectory distributions forces us to take into account pairs of trajectories and the possible correlations among them. The correlations are particularly important for $M^{\mathrm{d}}(t)$, as we show in Sec. 2.6. On the other hand, in our discussion of the last chapter we established that for the calculation of $M^{\mathrm{nd}}(t)$ the two trajectories of the pair can be considered to be uncorrelated with respect to the perturbation, and the averages can be performed independently. Assuming in addition that the measure of the momentum set $\varepsilon_{\mathbf{p}}$ is small compared with that of $\mathcal{P}_1$ we can write

$$M^{\mathrm{nd}}(t) \approx \left|\bar{O}_0(t) + \bar{O}_1(t)\right|^2 . \tag{43}$$

Substituting Eqs. (28) and (39) into Eq. (43) we find after straightforward algebraic operations as a central result for the non-diagonal contribution to the LE

$$\begin{aligned} M^{\mathrm{nd}}(t) \approx\; & \left[e^{-\gamma t} - \left(1 - e^{-\gamma t}\right) e^{-\chi\gamma t}\right]^2 \\ & + 4\left(1 - e^{-\gamma t}\right) \cos^2\left(\frac{\Omega\gamma t}{2}\right) e^{-(1+\chi)\gamma t}. \end{aligned} \tag{44}$$

The non-vanishing mean value Ω of the perturbation renders this expression distinctly different from the standard non-diagonal (Fermi-golden-rule) contribution to the LE studied so far in the literature. In chapter 2.7 we study the emergence of the oscillatory character of $M^{\mathrm{nd}}(t)$ resulting from quantum interference between $O_0(t)$ and $O_1(t)$, while in Secs. 3 and 4 we discuss the implications for numerical simulations and possible experimental observations.

2.6. Diagonal contribution to the Loschmidt echo

To proceed with the calculation of the diagonal contribution to the LE, Eq. (43), we first need to specify the set $\varepsilon_{\mathbf{p}}$ such that two trajectories of time t, starting from the phase space points $(\mathbf{r}_0, \mathbf{p})$ and $(\mathbf{r}_0, \mathbf{p}' \in \varepsilon_{\mathbf{p}})$, stay "correlated" during time t. As in Sec. 2.2, it is convenient to work with polar coordinates, $\mathbf{p} = (p, \theta)$ and $\mathbf{p}' = (p', \theta')$, in which the set $\varepsilon_{\mathbf{p}}$ can be defined as follows: for every $\mathbf{p}' \in \varepsilon_{\mathbf{p}}$ one has $|p' - p| \lesssim \Delta p$ and $|\theta' - \theta| \lesssim \Delta\theta$. In turn, Δp and $\Delta\theta$ are subject to the requirement that the two trajectories stay "close" to each other in phase space. Indeed, any two "correlated" trajectories must have the same number of collisions with the billiard boundary. This condition leads to $|p' - p| t/m \lesssim l_{\mathrm{f}}$. Moreover, the two trajectories must also have the same number of collisions with $\mathcal{B}_1$. The spatial separation between the two trajectories at the first collision with the boundary is approximately given by $|\theta' - \theta| l_{\rm f}$. The condition that after time t this separation is smaller that the size w of $\mathcal{B}_1$ is $|\theta' - \theta| l_{\rm f} \exp(\lambda t) \lesssim w$. Here we have used the property that for chaotic dynamics two arbitrary, initially close trajectories deviate exponentially from each over with a rate given by the average Lyapunov exponent λ. Thus, we can estimate the measure of the $\varepsilon_{\mathbf{p}}$-set to be

$$\Delta p = \frac{m l_{\rm f}}{t} \quad \text{and} \quad \Delta\theta = \frac{w}{l_{\rm f}} \exp(-\lambda t)\,. \tag{45}$$

Using this quantitative description of $\varepsilon_{\mathbf{p}}$ for the evaluation of Eq. (43) we obtain for the diagonal contribution to the LE

$$\begin{aligned} M^{\rm d}(t) = &\int_{\mathcal{P}_1} d\mathbf{p} W_0(\mathbf{p}) \int_{p-\Delta p}^{p+\Delta p} dp' p' \int_{\theta-\Delta\theta}^{\theta+\Delta\theta} d\theta' W_0(\mathbf{p}') \\ &\times \exp\left\{ \frac{i}{\hbar} \left[p' \Delta L(\mathbf{r}_0, p't, \theta') - p\Delta L(\mathbf{r}_0, pt, \theta) \right] \right\}. \end{aligned} \tag{46}$$

We now argue that for boundary deformations of moderate strength the exponent in the integrand on the right hand side of Eq. (47) can be neglected. The argument of the exponent is given by the total differential of the function $p\Delta L(\mathbf{r}_0, pt, \theta)$, and therefore its absolute value can be bounded by

$$\left| \frac{(p'-p)\Delta L}{\hbar} + \frac{p(\theta'-\theta)}{\hbar} \frac{\partial \Delta L}{\partial \theta} \right| \lesssim \left| \frac{\Delta p \Delta L}{\hbar} \right| + \left| \frac{p\Delta\theta}{\hbar} \frac{\partial \Delta L}{\partial \theta} \right|. \tag{47}$$

Here we have used that, as discussed in Sec. 2.3, ΔL is independent of p at fixed N. Then

$$\frac{\Delta p \Delta L}{\hbar} \sim \frac{\Delta p}{\hbar} \langle u \rangle \gamma t = \frac{l_{\rm f}}{l_{\rm d}} \Omega\,, \tag{48}$$

and

$$\frac{p\Delta\theta}{\hbar} \frac{\partial \Delta L}{\partial \theta} = \frac{p\Delta\theta}{\hbar} \sum_{j=1}^{N} \left(\frac{\partial u}{\partial \vartheta_j} \frac{\partial \vartheta_j}{\partial \theta} + \frac{\partial u}{\partial \xi_j} \frac{\partial \xi_j}{\partial \theta} \right) \sim \Delta\theta\, C e^{\lambda t} = \frac{w}{l_{\rm f}} C\,, \tag{49}$$

where we have introduced the dimensionless quantity

$$C = \frac{1}{\lambda_{\rm B}} \left\langle \frac{\partial u}{\partial \vartheta} \right\rangle + \frac{l_{\rm f}}{\lambda_{\rm B}} \left\langle \frac{\partial u}{\partial \xi} \right\rangle. \tag{50}$$

This implies that the exponent in Eq. (47) is smaller that unity if $\Omega \lesssim l_{\rm d}/l_{\rm f}$ and $C \lesssim l_{\rm f}/w$. Since the ratios $l_{\rm d}/l_{\rm f}$ and $l_{\rm f}/w$ are assumed to be large, the above inequalities hold for a wide range of deformations. (Note that for the piston-like deformation, Eq. (37), $\Omega = \pi h/2\lambda_{\rm B}$ and $C = 0$, and hence the exponent is small if $h \lesssim \lambda_{\rm B} l_{\rm d}/l_{\rm f}$.)

Neglecting the exponent in Eq. (47) we obtain

$$\begin{aligned} M^{\rm d}(t) &\approx \int_{\mathcal{P}_1} d\mathbf{p} W_0(\mathbf{p}) \int_{p-\Delta p}^{p+\Delta p} dp' p' \int_{\theta-\Delta\theta}^{\theta+\Delta\theta} d\theta' W_0(\mathbf{p}') \\ &\approx 4\Delta p \Delta\theta \int_{\mathcal{P}_1} d\mathbf{p} p W_0^2(\mathbf{p})\,. \end{aligned} \tag{51}$$

In the second line of this equation we have taken into account that $\Delta p \ll p$ and $\Delta\theta \ll 1$ for times t much longer than the dwell time $t_{\rm d}$. Under the assumption (26) of a "semiclassical" initial wave packet, the integral over p in Eq. (52) is dominated by the contribution around p_0 and we find

$$M^{\rm d}(t) \approx \frac{2mw}{\pi p_0 t}\left(\frac{\sigma}{\lambda_{\rm B}}\right)^2 \left(1-e^{-\gamma t}\right) e^{-\lambda t}. \tag{52}$$

We note that the exponential dependence of $M^{\rm d}$ on λt does not contain the perturbation and arises from a classical probability distribution, as in the standard Lyapunov regime [5]. The dependence with respect to the perturbation extent, w, appears in the prefactor and through the measure $(1-\exp(-\gamma t))$ of the ensemble Θ_1 corresponding to trajectories that hit $\mathcal{B}_1$ before t.

2.7. Decay regimes of the Loschmidt echo

According to Eq. (40) the full LE $M(t)$ is the sum of the non-diagonal and diagonal contributions, $M^{\rm nd}(t)$ and $M^{\rm d}(t)$, given by Eqs. (45) and (52) respectively. We first argue that, unlike in the case of a global Hamiltonian perturbation, *the non-diagonal contribution will typically dominate over the diagonal term.* The most favorable regime to observe the diagonal term would be that of a strong perturbation. It will dominate over its non-diagonal counterpart only if $\lambda < 2\gamma$. Since $\lambda - \gamma = h_{\rm KS} > 0$ (with $h_{\rm KS}$ the Kolmogorov-Sinai entropy of the chaotic repellor [26]) we see that $M^{\rm d}(t)$ will prevail over $M^{\rm nd}(t)$ when $2h_{\rm KS} < \lambda$. Taking into account that $h_{\rm KS} = \lambda$ for a close system, we see that only relatively open cavities would allow to observe $M^{\rm d}(t)$. Hence for further analysis of the LE decay we mainly focus on the non-diagonal contribution $M^{\rm nd}(t)$.

According to Eq. (45) three different decay regimes can be distinguished asymptotically in the long time limit, depending on the value of the deformation strength χ:

$$M^{\rm nd}(t) \sim \begin{cases} e^{-2\chi\gamma t}, & \chi < 1 \quad \text{(FGR)}; \\ 4e^{-2\gamma t}\cos^2\left(\dfrac{\Omega\gamma t}{2}\right) + e^{-4\gamma t}, & \chi \approx 1 \quad \text{(oscillatory)}; \\ e^{-2\gamma t}, & \chi > 1 \quad \text{(escape-rate)}. \end{cases} \tag{53}$$

We emphasize that Eq. (53) holds only if the conditions (7) and (26) are satisfied, i.e.

$$\lambda_{\rm B} \ll \sigma \ll \sqrt{\lambda_{\rm B} l_{\rm L}}\ , \tag{54}$$

where $l_{\rm L} = p_0/m\lambda$ is the Lyapunov length. Figure 3 illustrates these three decay regimes in the whole range from weak to strong perturbation strength χ for the case of the piston-like deformation (see Eq. (37) and App. Appendix B). For weak perturbation, the exponential decay depends on χ, in analogy to the Fermi-golden-rule regime found for global perturbations, but dressed in the present case with γ that provides a measure of the fraction of phase-space affected by the boundary deformation. In the opposite limit of strong perturbation, $\chi > 1$, we recover the escape-rate dominated decay reported previously [22].

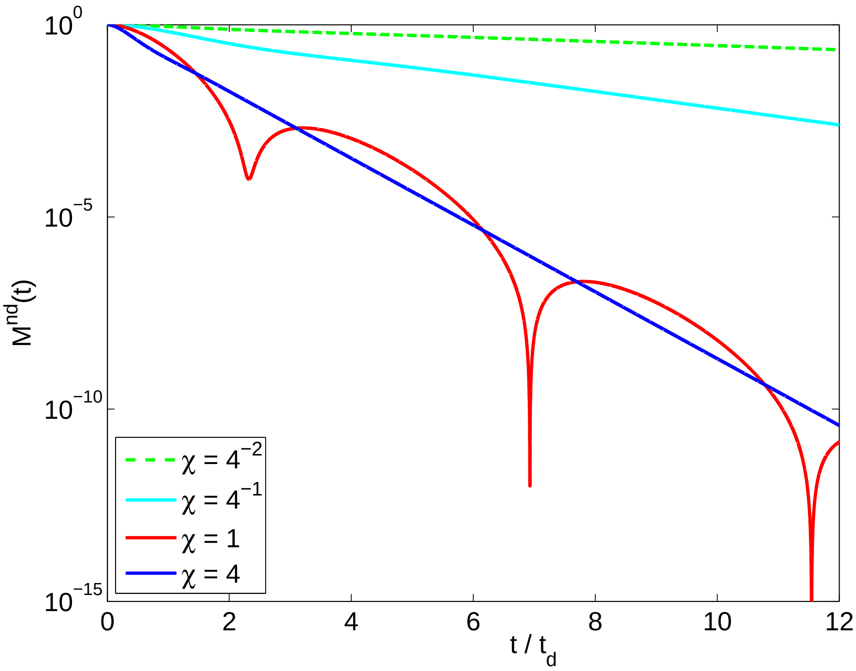

Figure 3. Decay regimes for the Loschmidt echo in a chaotic billiard due to a piston-like boundary deformation (see Appendix Appendix B). The non-diagonal contribution (Eq. (45)) governing the decay of the Loschmidt echo is depicted as a function of time in units of dwell time $t_{\rm d} = 1/\gamma$ for different values of the perturbation strength χ (Eq. (38)) corresponding to the Fermi-golden-rule ($\chi = 4^{-2}$ and $\chi = 4^{-1}$ curves), oscillatory ($\chi = 1$ curve), and escape-rate ($\chi = 4$ curve) regime (see Eq. (53)). Note that for a piston-like deformation Ω is uniquely determined by χ according to Eq. (B.3).

Most interestingly, for intermediate perturbation strengths we find oscillations in the echo with amplitudes scanning several orders of magnitude, superimposed on an overall exponential decay. In other words, for a fixed time t and starting in a minimum, the LE can increase by orders of magnitude upon varying the frequency of these oscillations. The frequency is given by the product of a classical quantity, the escape rate, and a quantity incorporating quantum interference, namely the mean value $\Omega = \langle u \rangle / \lambda_{\rm B}$ of the deformation function in units of the de Broglie wave length. The oscillation $\cos(\Omega\gamma t/2)$ can be interpreted as reflecting (constructive and destructive) interference from different pairs of paths, one pair not hitting $\mathcal{B}_1$ and the other hitting it on average γt times (and thus acquiring an extra phase of the order Ω per hit). While we argued before that $M^{\rm d}(t)$ will in general be dominated by $M^{\rm nd}(t)$, it is clear that the former will smooth out the big dips of the latter.

3. Decay oscillations and numerical simulations

In order to support our semiclassical predictions we present in this chapter numerical quantum mechanical calculations for a local perturbation. We use the Trotter-Suzuki algorithm [30, 31] to simulate the dynamics of a Gaussian wave packet inside a desymmetrized diamond billiard (DDB). The DDB is defined as a fundamental domain of the area confined by four intersecting disks of radius R centered at the verteces of a square. We denote the length of the largest straight segment of the DDB by L (see Fig. 4). As proved in Ref. [27], the DDB is fully chaotic and thus has been previously considered for studying aspects of quantum chaos [28].

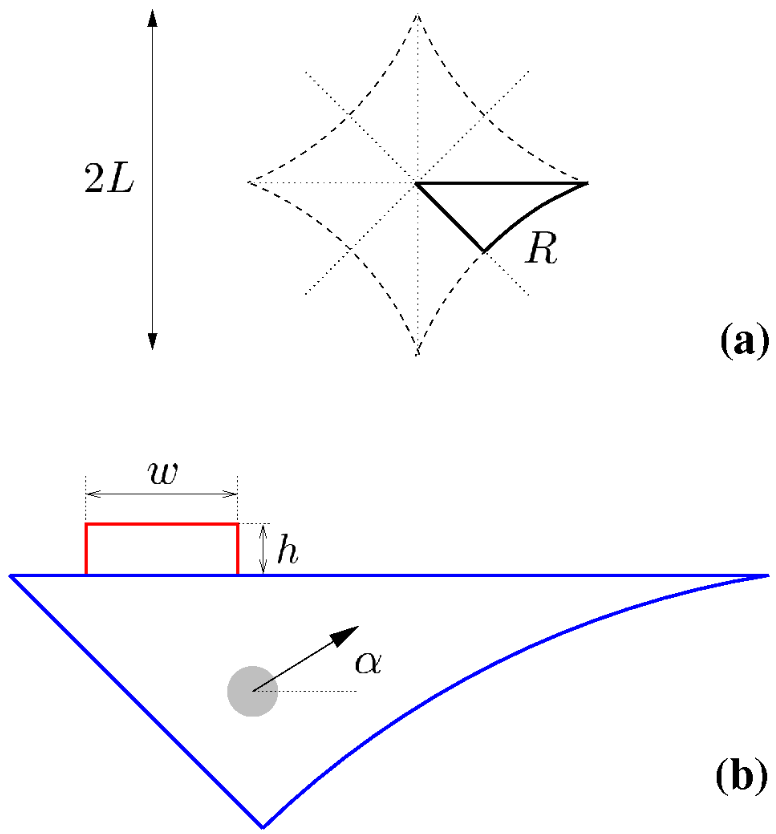

Figure 4. Desymmetrized diamond billiard: (a) the fundamental domain of the four-disk billiard, (b) the initial wave packet (with momentum enclosing an angle α with the horizontal) in the case of a local piston-like boundary deformation (defined by a width w and displacement h).

Our semiclassical analysis is valid for an arbitrarily shaped local perturbation acting on a region $\mathcal{B}_1$ (of width w) of the boundary. A perturbation with the shape of a circular segment was used in Ref. [22]. In our present numerical simulations we chose a piston-like perturbation (Fig. 4b), for which analytical results can be readily obtained (see Eq. (37) and Appendix Appendix B).

3.1. Strong deformation

In Fig. 5 we present the LE decay for a DDB with $L = 1000$, $R = 1311$ (in units of the lattice spacing of the underlying tight-binding model) and a piston-like perturbation. The piston displacements are $h = 9$ and $h = 10$, corresponding to $\chi = 12$ and $\chi \approx 14.8$

respectively. The initial wave packet is given by $\lambda_{\mathrm{B}} = 3$ and $\sigma = 8$. Its momentum direction is chosen to be parallel to the longest straight segment of the DDB ($\alpha = 0$ in Fig. 4.b), but we have verified that the LE decay rate is independent of α ‖. The numerically obtained LE curve decays exponentially for times t up to $4t_{\mathrm{d}}$ before turning over to a regime with strong irregular fluctuations around a saturation value [1]. For the present geometry the dwell time is $t_{\mathrm{d}} = 1/\gamma = (P/w)t_{\mathrm{f}} \approx 18.7\, t_{\mathrm{f}}$. The dashed straight line shows the trend of the semiclassically predicted decay, $\exp(-2\gamma t)$ (with γ obtained from Eq. (22)), which is well confirmed by the numerics. The shift in time of the numerically found exponential decay curve with respect to the dashed line depends on the position and momentum of the initial wave packet and is determined by the time scale until a corresponding distribution of classical particles is randomized.

Our results in the strong perturbation regime are in agreement with those of Ref. [22], thus supporting our theoretical predictions of Section 2, namely that in the limit of large χ the long-time LE decay only depends on the length w of the perturbed boundary segment, and neither on the shape, position or size of the perturbation, nor on the momentum direction of the initial wave packet.

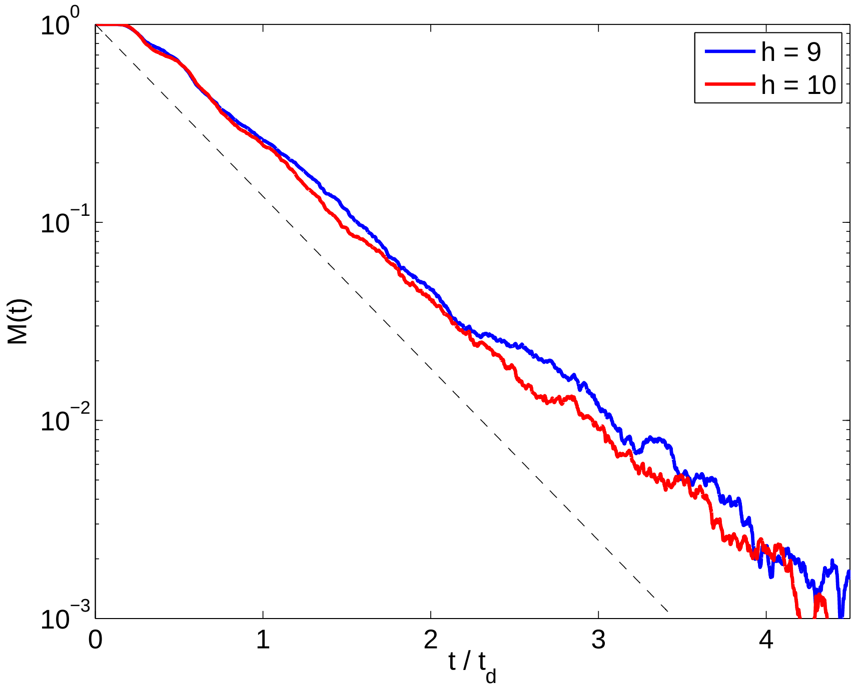

Figure 5. Loschmidt echo decay in the DDB for two different values of the displacement h of the piston-like deformation (see Fig. 4) and fixed width $w = 120$ of the perturbation region. The other system parameters are $\lambda_{\mathrm{B}} = 3$, $\sigma = 8$, $L = 1000$, and $R = 1311$. The time t is given in units of the dwell time $t_{\mathrm{d}} = 1/\gamma$. The dashed straight line shows the trend of the semiclassical prediction, $\exp(-2\gamma t)$, for the time decay, with γ given by Eq. (22).

‖ We exclude initial conditions for which the wave packet hits the perturbation before having considerably explored the allowed phase space.

3.2. Intermediate deformation strength

Fig. 6 shows our numerical results for the LE for a DDB with same paramters as in Fig. 5 and a piston-like perturbation with displacement $h = 3$ chosen to be in the regime of intermediate perturbation strength ($\chi \simeq 1$). The initial wave packet has $\sigma = 3$, and three different wavelenghts ($\lambda_{\rm B} = 2.8$, 3.0 and 3.2) are considered. We clearly see that the decay is different from that of the strong perturbation regime. However, the oscillations of Eq. (53) and Fig. 3 are not visible.

Such an outcome is not surprising since the numerical simulations of Fig. 6 do not fulfill the inequality of Eq. (26). That is, the initial wave packets that we can simulate are not sufficiently narrow such that the p integrals in Eqs. (23) and (24) would be given by the contribution around p_0. On the other hand, the above mentioned restriction on Eq. (26) can be easily lifted in our semiclassical approach in order to make a comparison with our numerics.

Instead of using the asymptotic form of the Bessel function I_0 (like in Sec. 2.2) we can write $O_0(t)$ as an integral over the dimensionless momentum variable $z = p/p_0$,

$$O_0(t) \approx \frac{2\sigma^2}{{\lambda_{\rm B}}^2} \int_0^\infty dz z \exp\left[-\gamma t z - \frac{\sigma^2}{{\lambda_{\rm B}}^2}(z^2+1)\right] I_0\left(\frac{2\sigma^2}{{\lambda_{\rm B}}^2} z\right) . \tag{55}$$

The average value of Eq. (39) was obtained under the assumption $p \simeq p_0$. Taking now into account the p-dependence of the average value and keeping, as in the previous case, the explicit form of I_0 we have

$$\begin{aligned} O_1(t) \approx & \frac{2\sigma^2}{{\lambda_{\rm B}}^2} \int_0^\infty dz z \left(1 - e^{-\gamma t z}\right) \\ & \times \exp\left[-\frac{\sigma^2}{{\lambda_{\rm B}}^2}(z^2+1) + i\Omega\gamma t z^2 - \chi\gamma t z^3\right] I_0\left(\frac{2\sigma^2}{{\lambda_{\rm B}}^2} z\right) . \end{aligned} \tag{56}$$

The numerical integrations of Eqs. (55) and (57), together with (43), allow to obtain $M^{\rm nd}(t)$ for a wider range of parameters than the approximation of Eq. (45). That is, for $\lambda_{\rm B} \lesssim \sigma \ll \sqrt{\lambda_{\rm B} l_{\rm L}}$ instead of the condition given by Eq. (54). The results, for the same system parameters than Fig. 6 ($\sigma = 8$, $h = 3$, and $\lambda_{\rm B} = 2.8$, 3.0, and 3.2) are presented in Fig. 7 $\mathcal{P}$. The semi-quantitative agreement between the two sets of curves representing the fully numerical and the semiclassical approaches is evident. From such an agreement we draw the following two important conclusions: **(i)** the semiclassical approximation correctly captures the physics of the LE decay, and **(ii)** *the broadening of the momentum distribution of the initial Gaussian wave packet* (or, in other words, the increase of the $\lambda_{\rm B}/\sigma$ ratio) *results in smearing out the oscillatory structure of the LE decay curves for moderate perturbation strengths* ($\chi \simeq 1$).

$\mathcal{P}$ In deriving Eqs. (55) and (57) we assumed the exponential, $\exp(-\gamma t)$, decay of classical probability density in the related open billiard obtained from the original one by removing the deformation-affected boundary segment. This assumptions is only valid for times t much longer that some t_0 defined as the time during which the initial localized probability distribution gets randomized over the billiard area. There is no LE decay for $t < t_0$; for the system parameters used in our numerical simulations $t_0 \approx 0.2\, t_{\rm d}$. Therefore, in comparing the numerical results with the analytical predictions one has to make the following “time shift”: $t \to t - t_0$ in Eqs. (55) and (57), while $M(t) = 1$ for $t < t_0$.

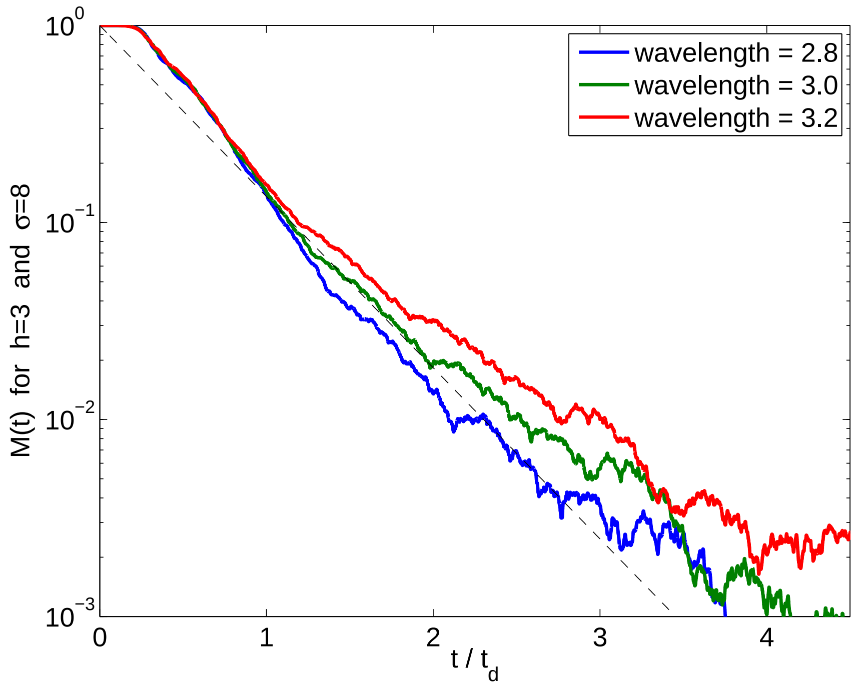

Figure 6. Numerically obtained time decay of the LE in a DDB due to a piston-like boundary deformation. The solid curves correspond to three different wavelengths $\lambda_{\rm B} = 2.8$, 3.0, and 3.2. The initial wave packet size is $\sigma = 8$. The deformation is characterized by the piston displacement $h = 3$ and width $w = 120$, see Appendix Appendix B. The DDB is defined by $L = 1000$ and $R = 1311$, see Fig. 4a. The time t is given in units of the dwell time $t_{\rm d} = 1/\gamma$. The dashed line corresponds to the exponential decay with the rate 2γ.

3.3. Onset of decay oscillations

In order to study the onset of the decay oscillations exhibited in Fig. 3, we consider different $\lambda_{\rm B}/\sigma$ ratios. Figure 8 depicts $M^{\rm nd}(t)$, obtained from Eqs. (55)-(57), for the same piston displacement ($h = 3$) and de Broglie wavelengths ($\lambda_{\rm B} = 2.8$, 3.0, and 3.2) of Fig. 7, but for a broader initial wave packet ($\sigma = 16$). The oscillations of the LE curves become more and more pronounced upon further decreasing the ratio $\lambda_{\rm B}/\sigma$ (keeping χ constant). In the limit $\lambda_{\rm B}/\sigma \to 0$ the overlaps $O_0(t)$ and $O_1(t)$ converge to their limiting values (28) confirming the results and conclusions of Section 2.

The maximum separation of scales we could attain in our numerical simulations was $\lambda_{\rm B} : \sigma : \sqrt{\lambda_{\rm B} l_{\rm L}} \sim 1 : 4 : 4^2$. Such a scale separation, as it is clear from Figs. 6-8, does not allow for resolving the fully developped oscillatory structure of the LE decay. It is easy to estimate that by decreasing the ratio $\lambda_{\rm B}/\sigma$ by a factor n iwill lead to an increase in computational time by the factor n^6 [+]. This makes it quite difficult to numerically

[+] Scaling $\sigma \to n\sigma$ also requires $l_{\rm L} \to n^2 l_{\rm L}$ to keep the ratio $\sigma/\sqrt{\lambda_{\rm B} l_{\rm L}}$ unchanged. This in turn is equivalent to increasing the linear size of the billiard n^2 times. The increase of the number of the computational grid points is then given by the factor n^4, and the number of time steps to propagate the wave function through the same total time multiplies by the factor n^2. This gives the overall factor

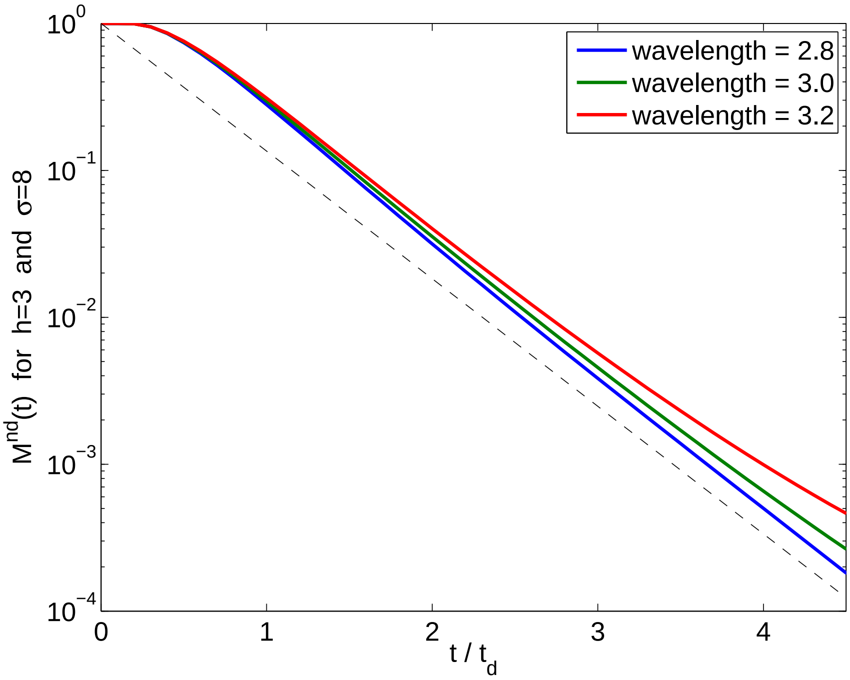

Figure 7. The LE time decay due to a piston-like deformation calculated according to Eqs. (43), (55) and (57), cf. Fig. 6. The initial wave packet size is $\sigma = 8$. The solid curves correspond to three different wavelengths $\lambda_{\rm B} = 2.8$, 3.0, and 3.2. The deformation is characterized by the piston displacement $h = 3$. The time t is given in units of the dwell time $t_{\rm d} = 1/\gamma$. The dashed line corresponds to the exponential decay with the rate 2γ.

reproduce the oscillatory decay regime predicted in Section 2.

Another (and probably more important) obstacle on the way to numerically reproducing the oscillatory decay regime is the early saturation of the LE to its quantum saturation value $M_{\rm s}$. The latter is inversely proportional to the size of the effective Hilbert space (or the size of the computational grid), making the saturation time increase only logarithmically with the increase in the computational time. In our present numerical studies the noise related to the LE saturation sets in already at values of the LE of $M \sim 10^{-3}$, whereas, as it is obvious from Figs. 3 and 8, the first minimum of the $M(t)$ in the oscillatory regime occurs for values below 10^{-3}.

Establishing the correspondence between the fully numerical and semi-analytical approaches in the regime of common applicability has been a helpful step towards the validation of our semiclassical calculations. As we discuss in the next section, unlike present numerical calculations, experiments may be designed to reach the LE regime where the novel oscillations should be found.

n^6 for the code running time.

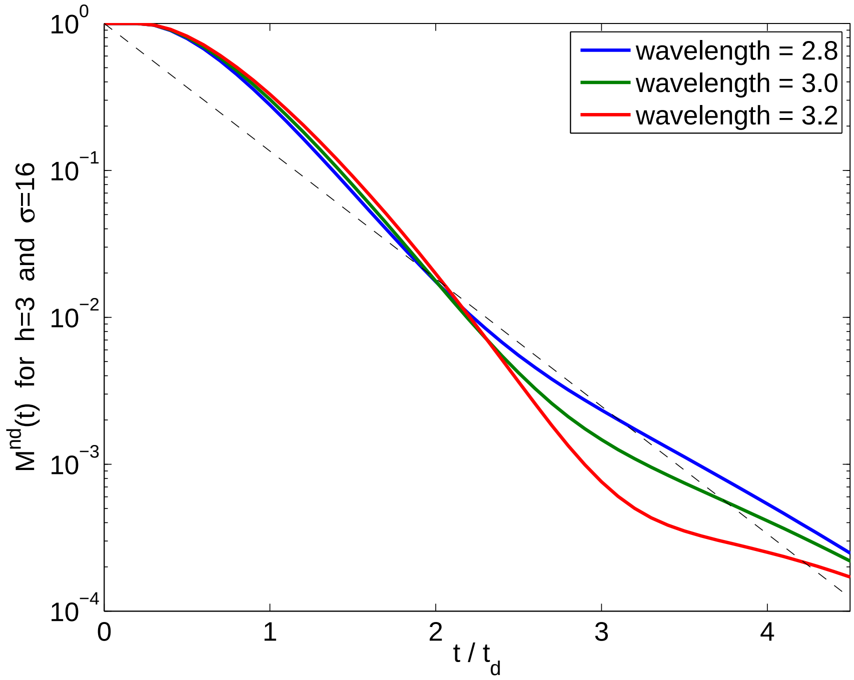

Figure 8. Non-diagonal contribution to the LE due to a piston-like deformation calculated according to Eqs. (43), (55) and (57). The initial wave packet size is $\sigma = 16$. The solid curves correspond to three different wavelengths $\lambda_B = 2.8$, 3.0, and 3.2. The deformation is characterized by the piston displacement $h = 3$. The time t is given in units of the dwell time $t_d = 1/\gamma$. The dashed line corresponds to the exponential decay with the rate 2γ.

4. Decay oscillations: microwave and cold atom cavities

Experiments of the LE * are of foremost importance since they render crucial information about the physical system and its decoherence mechanisms. While the examples discussed in the introduction show that the agreement between the semiclassical theory of the LE and numerical simulations is quite successful, the situation is less satisfactory concerning experiments.

LE experiments were first performed on nuclear spins of organic molecules using NMR techniques [4, 33]. The decay of the polarization was found to be quite insensitive to the coupling to external degrees of freedom or the precision of the reversal. The Gaussian decay of the experimentally measured LE is at odds with the one-body semiclassical theory, and many-body aspects of the problem have been pointed to be at the origin of such a behavior [34, 35].

With regard to the LE for local boundary perturbations in the escape-rate regime we proposed in Ref. [22] a principle experimental scheme for measuring the LE decay based on a ballistic electron cavity with a small ferromagnet attached acting as the local perturbation. Such a setting provides a link between spin relaxation in a mesoscopic

* For a recent account see Sec. 9 in Ref. [6]

cavity and LE decay. Here we address two further experimental settings which appear suitable for a measurement of the echo decay.

The scattering fidelity, defined as a cross correlation of scattering matrix elements, has been recently measured in microwave cavities [36]. When appropriate ensemble and/or energy averages are taken it gives a good representation of the average fidelity amplitude. From the amplitudes measured independently for the unperturbed and perturbed system the fidelity, respectively, the LE can be constructed. The scattering fidelity measurements (for a global perturbation in the microwave cavity) are in good agreement with calculations in the perturbative and golden-rule regime, but accessing the longer timescales of the Lyapunov decay regime remains an experimental challenge. However, the corresponding (escape-rate) decay regime for local perturbations may be easier reached experimentally. Moreover, microwave billiards appear to be rather suited to investigate local boundary perturbations, since the piston-type deformation suggested in the present paper, can be directly realized in a microwave billiard setup. The width of the piston determines the exponent of the LE time decay. Furthermore, by moving the piston the perturbation strength χ, and thereby the frequency of the LE oscillations, Ω (see Eq. (B.3)), can be directly controlled and tuned. Hence, ny devising sufficiently large microwave cavities to approach the semiclassical limit it seems promising to experimentally reach both, the oscillatory LE regime for intermediate χ and the escape-rate regime for larger χ.

Studying quantum chaos in the laboratory by recreating a delta-kicked harmonic oscillator in an ion trap was proposed a decade ago by Gardiner and collaborators [37], and a number of fruitful approaches have since then been developed and successfully realized using ultra-cold atoms confined to optical billiards [38]. For instance, the decay of quantum correlations has been measured by echo spectroscopy on ultra-cold atoms using the detuning of the trapping laser as a perturbation [39]. Below we focus on the time evolution of clouds of ultra-cold atoms in optical billiards, and show that they provide a viable system for experimental investigation of different perturbations and various regimes of the LE decay. The perturbations can be global, such as in the cases previously studied, but also local. Since the large-scale separation of system parameters, given by the conditions (7) and (26), is attainable in these experimental systems we expect that the oscillatory decay regime predicted above can be reachable.

In a typical microwave echo (or Ramsey) spectroscopy experiment [39] a cloud of ultra-cold Rb atoms is loaded into an off-resonance optical trap. For the purpose of our study the role of the trap can be played by a hollow laser beam with the cross section corresponding to the geometry of a chaotic billiard of interest. The fabrication of such hollow laser beams, as well as the manipulation of atoms inside them, can now be performed with a high level of precision [40]. The atomic cloud, after being positioned inside the hollow beam in its focal plane and accelerated (or "kicked") as a whole to a nonzero average momentum, is let to evolve freely in an effectively two-dimensional billiard, see Fig. 9.

The Rb atoms used in echo experiments [39] are initially prepared in a quantum

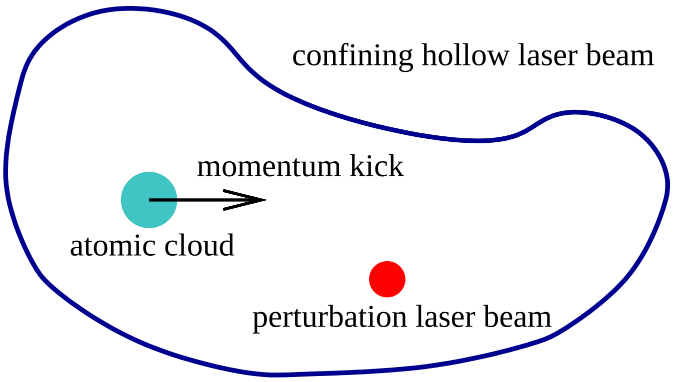

Figure 9. Atom-optics billiard: a sketch of the focal plane of the hollow laser beam.

state Ψ_0 equal to a direct product of an internal atomic state $|s\rangle$ and a spatial state described by a wave function $\phi_0(\mathbf{r})$, i.e. $\Psi_0 = |s\rangle \otimes \phi_0(\mathbf{r})$. The internal state evolves in a coherent superposition of the two hyperfine sub-states, denoted by $|\downarrow\rangle$ and $|\uparrow\rangle$, of the ground state of rubidium. The $|\downarrow\rangle$-component of the total wave function of an atom experiences a laser field potential $V_\downarrow(\mathbf{r})$ which is, in general, different from the potential $V_\uparrow(\mathbf{r})$ exerted by the same laser on the $|\uparrow\rangle$-component. The relative difference between the two optical potentials is given by the ratio $\omega_{\mathrm{HF}}/\Delta_{\mathrm{L}}$, where $\hbar\omega_{\mathrm{HF}}$ is the energy of the hyperfine splitting of the ground state, and Δ_{L} is the laser detuning from the frequency of the transition between the ground state and the first allowed excited state of the Rb atom. The application of a sequence of $\pi/2$ microwave pulses during the time evolution of the atoms, followed by a measurement of the populations of the $|\downarrow\rangle$- and $|\uparrow\rangle$-sub-states at the end of the evolution, allows one to determine the LE (corresponding to the spatial wave function $\phi_0(\mathbf{r})$) due to the difference between the potentials $V_\downarrow(\mathbf{r})$ and $V_\uparrow(\mathbf{r})$ as a function of the evolution time.

In order to measure the LE decay due to local perturbations two different lasers have to be used. The first laser is to produce the confining hollow beam with the cross section of a desired (billiard) geometry, and has to be tuned as to exert approximately the same potential $V_{\mathrm{bill}}(\mathbf{r})$ on the both $|\downarrow\rangle$- and $|\uparrow\rangle$-sub-states. The beam of the second laser plays a role of the local Hamiltonian perturbation. It has to be placed inside (and aligned with) the hollow beam of the first confining laser, and its width should be much smaller than the linaer scale of the billiard (see Fig. 9). The frequency of this second laser (and perhaps its position inside the billiard) determines the perturbation strength χ. Altering this frequency changes the difference between the potentials $\delta V_\downarrow(\mathbf{r})$ and $\delta V_\uparrow(\mathbf{r})$, produced by the second laser and acting differently on the $|\downarrow\rangle$- and $|\uparrow\rangle$-substates, respectively. Thus, an echo spectroscopy experiment performed in such a system would measure the LE decay due to the difference of the atomic potentials $V_\downarrow(\mathbf{r}) = V_{\mathrm{bill}}(\mathbf{r}) + \delta V_\downarrow(\mathbf{r})$ and $V_\uparrow(\mathbf{r}) = V_{\mathrm{bill}}(\mathbf{r}) + \delta V_\uparrow(\mathbf{r})$; this difference is localized in an area much smaller than that of the billiard.

To date one is typically able to experimentally prepare and manipulate clouds of Rb atoms as cold as 1 μK. This temperature corresponds to the thermal speed of about 1.3

cm/sec. At the same time, by first placing the atoms inside a far-off-resonance dipole trap then moving the trap and finally switching it off one can accelerate the atomic cloud as a whole up to 10 *cm/sec*. Such a momentum kick can nowadays be easily realized in a laboratory, and does not significantly increase the temperature of the atoms. As a result one obtains a cloud of atoms moving as a whole with an average momentum that corresponds to a de Broglie wave length $\lambda_{\rm B} \sim 10\,nm$. The dispersion of the atomic cloud can be shrunk to $\sigma \approx 1\,\mu m$. Under this conditions the number of Rb atoms composing the cloud can reach 10^5 that is well sufficient for the Ramsey-spectroscopy-type measurements. The hollow laser beam, producing the billiard confinement, can reach $L \approx 1cm$ in linear size. Assuming the Lyapunov scale $l_{\rm L}$ of the billiard to be of the same order of magnitude as L one arrives at the following estimate for the scale separation of the system parameters:

$$\lambda_{\rm B} : \sigma : \sqrt{\lambda_{\rm B} l_{\rm L}} \sim 1 : 10^2 : 10^3, \tag{57}$$

which well satisfies the restriction given by Eq. (54). Under the conditions specified above one can control the atoms for up to 5 *secs* before the cloud gets significantly elongated in the axial direction of the hollow laser beam. Such a time allows a single atom to experience about 50 bounces with the billiard boundary, which according to our theory is sufficient for observing the LE decay regimes predicted in this work.

The above considerations show that atom-optics billiards constitute promising candidates for experimentally investigating different regimes of the LE decay due to local perturbations of the Hamiltonian, and in particular put in evidence the predicted decay oscillations.

5. Conclusions

In this work we have studied the time decay of the Loschmidt echo in quantum systems that are chaotic in the classical limit, due to Hamiltonian perturbations localized in coordinate space. We have provided the corresponding semiclassical theory of the LE for small coherent initial states evolving in two-dimensional chaotic billiards.

In addition to the FGR decay regime, which is well-known for the case of global Hamiltonian perturbations and is recovered in our theory for weak ($\chi < 1$) local perturbations, our analysis predicts two novel decay regimes that stem entirely from the local nature of the Hamiltonian perturbation, i.e. the *escape-rate* and *oscillatory* regimes. In the former regime, reached for strong ($\chi > 1$) perturbations, the LE decays exponentially in time with a rate equal to twice the escape rate from an open billiard with the "hole" at the place of the deformation. Hence the LE allows to mimic the decay behavior of a system without opening it. In this regime the LE decay rate is independent of the deformation strength χ. The oscillatory regime occurs for perturbations of intermediate ($\chi \simeq 1$) strength and marks the crossover between the FGR decay and the escape-rate saturation. There the LE oscillates wildly as a function of time while confined to an exponentially decaying envelope.

Other non-monotonous LE decays have been previously reported in the literature. A numerical analysis for the quantum kicked rotor showed also oscillations in the fidelity decay (see Fig. 9 in Ref. [41]) due to stable islands in the related classical mixed regular/chaotic phase space. Furthermore, in a different study fluctuations of the Lyapunov exponent in phase space may induce a double exponential decay of the typical LE that joins the standard Lyapunov regime for later times [13]. Studies of LE in a three-junction SQUID device using variations of the flux and/or junction capacitance yielded an exponential Lyapunov decay supperposed to strong oscillations of $M(t)$ [19]. While the origin of these oscillations has not been clarified yet, they might be related to the non-uniformity of the perturbation in phase-space. In these two latter cases the non-monotonous behavior is obtained for the regime of strong perturbation, unlike our case, where it appears from quantum interference when the non-diagonal term is dominant. Similar interferences, going beyond the standard Fermi-golden-rule, have been studied for the polarization decay in spin chains [29]. In that case the interference is between the Fermi-golden-rule contribution and the return correction from quantum diffusion, and a non-monotonous behavior of the polarization decay is obtained in the regime where the two contributions are of the same order.

We have also performed an extensive numerical study of the LE decay to support our semiclassical theory. To this end we have the simulated time evolution of initially small coherent states in the DDB. The role of the local Hamiltonian perturbation was played by a piston-like deformation of the billiard boundary. The results of our numerical simulations exhibit considerable agreement with the theoretical predictions. Our simulations clearly indicate the escape-rate decay regime of the LE for strong perturbations, and therefore complement and generalize the results of Ref. [22], in which a boundary deformation of a different shape has been considered. Since the parameters of our system do not provide the scale separation (Eq. (54)) necessary for obtaining the oscillatory decay regime we observe only precursors of the latter in our numerical simulations for the boundary deformations of intermediate strength. These numerical results perfectly agree with the predictions of our theory extended to cope with initial states given by Gaussian wave packets of a dispersion comparable with the de Broglie wavelength.

While the scale separation given by Eq. (54) is rather challenging to be satisfied numerically it can be naturally achieved in laboratory experiments with ultra-cold atoms confined to optical billiards. In this work we have proposed a laboratory set-up allowing one to investigate the LE decay from local Hamiltonian perturbations for a wide range of perturbation strengths, and to observe the three predicted decay regimes. We believe that the study of the LE decay due to local perturbations provides an example of physical problems for which capabilities of laboratory experiments go beyond those of numerical simulations.

Such experiments may also reveal weak-localization-type quantum corrections to the LE decay which are expected from an analysis [42] of loop corrections [43] beyond the semiclassical diagonal approximation.

Acknowledgments

The authors would like to thank Inanc Adagideli, Arnd Bäcker, Philippe Jacquod, Thomas Seligman and Steven Tomsovic for helpful conversations. Special acknowledgments go to Ilya Arakelyan for providing the authors with helpful information about state-of-the-art atom-optics experiments. This work has been supported by the Alexander von Humboldt Foundation (AG), the Vielberth foundation (RJ) and the Deutsche Forschungsgemeinschaft within FG 760 (RJ, KR) and GRK 638 (DW, KR).

Appendix A. Linearization of the action integral

Here we present the details of the expansion of the action integral (or the Hamilton principal function) around the central trajectory of the wave packet. This is generally an important aspect of the semiclassical approach to the LE that has so far been treated in a very approximate way [10].

As shown in Fig. 1, we consider a wave packet centered at $\mathbf{r}_0$ and localized at a small circular region of radius σ. The action integral $S_{\hat{s}}(\mathbf{r}, \mathbf{r}', t)$ along a trajectory $\hat{s}$ starting at a point $\mathbf{r}'$ within this circular region at time 0 and leading to $\mathbf{r}$ in a time t can be expanded as

$$\begin{aligned} S_{\hat{s}}(\mathbf{r}, \mathbf{r}', t) = S_s(\mathbf{r}, \mathbf{r}_0, t) + (\mathbf{r}' - \mathbf{r}_0) \cdot \left[\frac{\partial S_{\hat{s}}(\mathbf{r}, \mathbf{r}', t)}{\partial \mathbf{r}'} \right]_{\mathbf{r}'=\mathbf{r}_0} \\ + \frac{1}{2} (\mathbf{r}' - \mathbf{r}_0) \cdot \left[\frac{\partial^2 S_{\hat{s}}(\mathbf{r}, \mathbf{r}', t)}{\partial \mathbf{r}'^2} \right]_{\mathbf{r}'=\mathbf{r}_0} (\mathbf{r}' - \mathbf{r}_0) + \ldots . \end{aligned} \tag{A.1}$$

Here we assume that the trajectory $\hat{s}(\mathbf{r}, \mathbf{r}', t)$ converges to the central trajectory $s(\mathbf{r}, \mathbf{r}_0, t)$ as $\mathbf{r}'$ approaches $\mathbf{r}_0$. The dot denotes the scalar (as opposed to matrix) multiplication. Using the identity $\partial S_{\hat{s}}/\partial \mathbf{r}' = -\mathbf{p}_{\hat{s}}$, where $\mathbf{p}_{\hat{s}}$ denotes the initial momentum on the trajectory $\hat{s}(\mathbf{r}, \mathbf{r}', t)$, we rewrite Eq. (A.2) as

$$\begin{aligned} S_{\hat{s}}(\mathbf{r}, \mathbf{r}', t) = S_s(\mathbf{r}, \mathbf{r}_0, t) - \mathbf{p}_s \cdot (\mathbf{r}' - \mathbf{r}_0) \\ - \frac{1}{2} (\mathbf{r}' - \mathbf{r}_0) \cdot \left[\frac{\partial \mathbf{p}_{\hat{s}}}{\partial \mathbf{r}'} \right]_{\mathbf{r}'=\mathbf{r}_0} (\mathbf{r}' - \mathbf{r}_0) + \ldots . \end{aligned} \tag{A.2}$$

Note that in our notation $\mathbf{p}_{\hat{s}} \to \mathbf{p}_s$ as $\mathbf{r}' \to \mathbf{r}_0$, see Fig. 1. In order to truncate the expansion (A.3) at the term linear in $\mathbf{r}' - \mathbf{r}_0$, and therefore recover Eq. (6), the condition

$$\left| (\mathbf{r}' - \mathbf{r}_0) \cdot \left[\frac{\partial \mathbf{p}_{\hat{s}}}{\partial \mathbf{r}'} \right]_{\mathbf{r}'=\mathbf{r}_0} (\mathbf{r}' - \mathbf{r}_0) \right| \ll \hbar \tag{A.3}$$

must be satisfied for all points $\mathbf{r}'$ such that $|\mathbf{r}' - \mathbf{r}_0| \lesssim \sigma$.

To analyze Eq. (A.3) we introduce a system of relative coordinates moving along the central trajectory $s(\mathbf{r}, \mathbf{r}_0, t)$. Thus, for any time $\tau \in [0, t]$ the distance between the phase space points $(\mathbf{q}'_\tau, \mathbf{p}'_\tau)$ and $(\mathbf{q}_\tau, \mathbf{p}_\tau)$, belonging to the trajectory $\hat{s}(\mathbf{r}, \mathbf{r}', t)$ and $s(\mathbf{r}, \mathbf{r}_0, t)$ respectively, is given by $\mathbf{q}'_\tau - \mathbf{q}_\tau = (q^{\parallel}_\tau, q^{\perp}_\tau)$ and $\mathbf{p}'_\tau - \mathbf{p}_\tau = (p^{\parallel}_\tau, p^{\perp}_\tau)$, where the superscripts $\parallel$ and $\perp$ refer to the vector components parallel and perpendicular to $\mathbf{p}_\tau$.

(Note that in the current notation $\mathbf{q}_0 \equiv \mathbf{r}_0$, $\mathbf{q}'_0 \equiv \mathbf{r}'$, $\mathbf{q}_t = \mathbf{q}'_t \equiv \mathbf{r}$, $\mathbf{p}_0 \equiv \mathbf{p}_s$ and $\mathbf{p}'_0 \equiv \mathbf{p}_{\hat{s}}$.) Then

$$\left[\frac{\partial \mathbf{p}_{\hat{s}}}{\partial \mathbf{r}'}\right]_{\mathbf{r}'=\mathbf{r}_0} = \left(\begin{array}{cc} \partial p_0^{\|}/\partial q_0^{\|} & \partial p_0^{\|}/\partial q_0^{\perp} \\ \partial p_0^{\perp}/\partial q_0^{\|} & \partial p_0^{\perp}/\partial q_0^{\perp} \end{array}\right)_{(q_0^{\|},\, q_0^{\perp})=\mathbf{0}} . \tag{A.4}$$

For a billiard the off-diagonal partial derivatives can be neglected compared to the diagonal ones, so that condition (A.3) can be replaced by

$$\sigma^2 \left| \frac{\partial p_0^{\|}}{\partial q_0^{\|}} + \frac{\partial p_0^{\perp}}{\partial q_0^{\perp}} \right|_{(q_0^{\|},\, q_0^{\perp})=\mathbf{0}} \ll \hbar \, . \tag{A.5}$$

The first of the two derivatives in Eq. (A.5) is $\partial p_0^{\|}/\partial q_0^{\|} = -m/t$ for a particle of mass m in a billiard. To evaluate the second derivative we first linearize the trajectory $\hat{s}(\mathbf{r}, \mathbf{r}', t)$ around $s(\mathbf{r}, \mathbf{r}_0, t)$, so that $q_\tau^{\perp} \approx q_\tau^{\perp}(q_0^{\perp}, p_0^{\perp}, \tau)$. Therefore,

$$0 \equiv dq_t^{\perp} = \left(\frac{\partial q_t^{\perp}}{\partial q_0^{\perp}}\right)_{p_0^{\perp}} dq_0^{\perp} + \left(\frac{\partial q_t^{\perp}}{\partial p_0^{\perp}}\right)_{q_0^{\perp}} dp_0^{\perp} \, , \tag{A.6}$$

which leads to

$$\left(\frac{\partial p_0^{\perp}}{\partial q_0^{\perp}}\right)_{q_t^{\perp}} = -\frac{\left(\partial q_t^{\perp}/\partial q_0^{\perp}\right)_{p_0^{\perp}}}{\left(\partial q_t^{\perp}/\partial p_0^{\perp}\right)_{q_0^{\perp}}} \, . \tag{A.7}$$

The right hand side of Eq. (A.7) is given by the ratio of the two monodromy matrix elements. To facilitate our analytical presentation, we use here the monodromy matrix of the dynamics on Riemann surfaces of constant negative curvature ♯,

$$\left(\begin{array}{cc} \partial q_t^{\perp}/\partial q_0^{\perp} & \partial q_t^{\perp}/\partial p_0^{\perp} \\ \partial p_t^{\perp}/\partial q_0^{\perp} & \partial p_t^{\perp}/\partial p_0^{\perp} \end{array}\right) = \left(\begin{array}{cc} \cosh(\lambda t) & (m\lambda)^{-1}\sinh(\lambda t) \\ m\lambda \sinh(\lambda t) & \cosh(\lambda t) \end{array}\right), \tag{A.8}$$

with λ the Lyapunov exponent. For times longer than the Lyapunov time, $t \gg 1/\lambda$, we have $\partial p_0^{\perp}/\partial q_0^{\perp} \approx -m\lambda$, so that Eq. (A.5) can be replaced by

$$\sigma^2 m\lambda \ll \hbar \, . \tag{A.9}$$

In terms of the Lyapunov length $l_{\rm L} = (p/m)(1/\lambda)$, conveniently used for billiards, Eq. (A.9) then reads

$$\sigma \ll \sqrt{\frac{\hbar l_{\rm L}}{p}} \, . \tag{A.10}$$

The momentum uncertainty of a Gaussian wave packet of dispersion σ is $\hbar/\sigma$, so that $p \lesssim \hbar/\lambda_{\rm B} + \hbar/\sigma$, with $\lambda_{\rm B}$ the de Broglie wavelength. Therefore, condition (A.10) holds for every trajectory relevant for the wave packet propagation only if

$$\sigma \ll \sqrt{\frac{l_{\rm L}}{1/\lambda_{\rm B} + 1/\sigma}} \, . \tag{A.11}$$

The action integral expansion (6) requires condition (A.11) to be satisfied. We finally note that in the limit $\lambda_{\rm B} \ll \sigma$, which we utilize in Sec. 2, Eq. (A.11) simplifies to $\sigma \ll \sqrt{\lambda_{\rm B} l_{\rm L}}$.

♯ The dynamics of the motion on Riemann surfaces of constant negative curvature is known to be uniformly hyperbolic, with all trajectories possessing the same Lyapunov exponent.

Appendix B. Piston-like boundary deformation

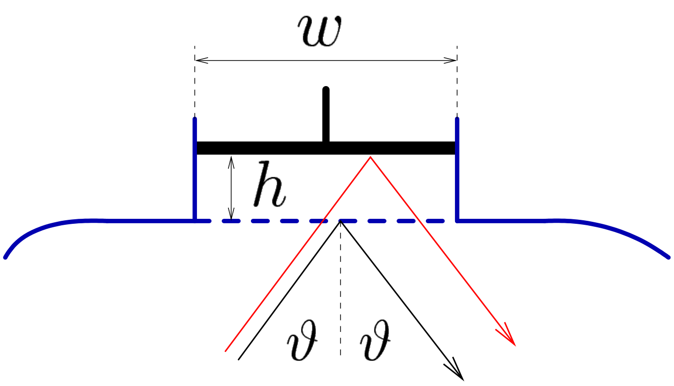

Figure B1. Piston-like boundary deformation.

In this appendix we explicitly compute as an example the length-difference function $u(\vartheta,\xi)$ of Eq. (29) for a piston-like local boundary deformation, see Fig. B1, which is also used in our numerics. We assume that the boundary of the unperturbed billiard possesses a straight segment of length w that gets "lifted" by the perturbation as if an imaginary "piston" was pulled out. We denote the piston displacement by h. Assuming h much smaller than the free flight path $l_{\rm f}$ of the trajectory hitting the deformation, we treat the unperturbed and perturbed trajectories to be parallel. Then the length difference $u(\vartheta,\xi)$ accumulated due to a single collision with the deformation-affected segment of the boundary is given by an expression analogous to Bragg's diffraction formula,

$$u(\vartheta,\xi) \approx 2h\cos\vartheta\,. \tag{B.1}$$

Here ϑ represents the collision angle as shown in Fig. B1. The length difference u can be considered independent of the collision coordinate ξ for deformations such that $h \ll w$.

Taking into account the probability distribution function of collision angles, Eq. (32), we have $\langle\cos\vartheta\rangle = \pi/4$ and $\langle\cos^2\vartheta\rangle = 2/3$. Consequently, the first two moments of the deformation function read

$$\langle u\rangle = \frac{\pi}{2}h \qquad \text{and} \qquad \langle u^2\rangle = \frac{8}{3}h^2. \tag{B.2}$$

We finally note that for the piston-like deformation

$$\Omega = \frac{\pi\sqrt{3}}{4}\chi^{1/2}\,, \tag{B.3}$$

i.e., the perturbation strength χ and frequency Ω are not independent.

[1] A. Peres, Phys. Rev. A **30**, 1610 (1984).
[2] M. A. Nielsen and I. L. Chuang, *Quantum computation and quantum information* (Cambridge University Press, Cambridge, New York, 2000).
[3] E. L. Hahn, Phys. Rev. **80**, 580 (1950); R. G. Brewer and E. L. Hahn, Sci. Am. **251**, 50 (1984).
[4] G. Usaj, H. M. Pastawski, P. R. Levstein, Mol. Phys. **95**, 1229 (1998).
[5] R. A. Jalabert and H. M. Pastawski, Phys. Rev. Lett. **86**, 2490 (2001).

[6] For a review see T. Gorin, T. Prosen, T. Seligman, and M. Znidaric, Phys. Rep. **435**, 33 (2006).
[7] Ph. Jacquod, P. G. Silvestrov, and C. W. J. Beenakker, Phys. Rev. E **64**, 055203(R) (2001).
[8] N. R. Cerruti and S. Tomsovic, Phys. Rev. Lett. **88**, 054103 (2002); J. Phys. A **36**, 3451 (2003).
[9] T. Prosen, T. H. Seligman, and M. Znidaric, Prog. Theor. Phys. Suppl. **150**, 200 (2003).
[10] F. M. Cucchietti, H. M. Pastawski, and R. A. Jalabert, Phys. Rev. B **70**, 035311 (2004).
[11] C. Petitjean and Ph. Jacquod, Phys. Rev. E **71**, 036223 (2005).
[12] W. Wang, G. Casati, B. Li, and T. Prosen, Phys. Rev. E **71**, 037202 (2005).
[13] P. G. Silvestrov, J. Tworzydlo, and C. W. J. Beenakker, Phys. Rev. E **67**, 025204(R) (2003).
[14] Y. Adamov, I.V. Gornyi, and A.D. Mirlin, Phys. Rev. E **67**, 056217 (2003).
[15] A. Iomin, Phys. Rev. E **70**, 026206 (2004).
[16] F. M. Cucchietti, H. M. Pastawski, and D. A. Wisniacki, Phys. Rev. E **65**, 045206(R) (2002).
[17] D. A. Wisniacki, E. G. Vergini, H. M. Pastawski, and F. M. Cucchietti, Phys. Rev. E **65**, 055206(R) (2002).
[18] F. M. Cucchietti, C. H. Lewenkopf, E. R. Mucciolo, H. M. Pastawski, and R. O. Vallejos, Phys. Rev. E **65**, 046209 (2002).
[19] E.N. Pozzo and D. Domínguez, Phys. Rev. Lett. **98**, 057006 (2007).
[20] J. Vanicek, Phys. Rev. E **70**, 055201(R) (2004).
[21] M. V. Berry, Proc. R. Soc. London A **400**, 229 (1985).
[22] A. Goussev and K. Richter, Phys. Rev. E **75**, 015201(R) (2007).
[23] see e.g., M. Brack and R. K. Bhaduri, *Semiclassical Physics* (Addison-Wesley, Reading, 1997).
[24] O. Legrand and D. Sornette, Phys. Rev. Lett. **66**, 2172 (1991), and references therein.
[25] H. U. Baranger, R. A. Jalabert, and A. D. Stone, Chaos, **3**, 665 (1993), and references therein.
[26] H. Kantz and P. Grassberger, Pysica D **17**, 75 (1985); J.-P. Eckmann and D. Ruelle, Rev. Mod. Phys. **57**, 617 (1985).
[27] A. Krámli, N. Simányi, and D. Szász, Comm. Math. Phys. **125**, 439 (1989).
[28] S. Müller, Eur. Phys. J. B **34**, 305 (2003); O. Zaitsev, D. Frustaglia, and K. Richter, Phys. Rev. Lett. **94**, 026809 (2005), Phys. Rev. B **72**, 155325 (2005).
[29] E. Rufeil Fiori, H. M. Pastawski, Chem. Phys. Lett. **420**, 35 (2006).
[30] H. De Raedt, Annu. Rev. Comput. Phys. **4**, 107 (1996).
[31] F. M. Cucchietti, Ph.D. thesis, Universidad Nacional de Córdoba, Argentina, 2004, e-print: quant-ph/0410121v1.
[32] S. F. Nielsen, P. Dahlqvist, and P. Cvitanović, J. Phys. A **32**, 6757 (1999).
[33] H. M. Pastawski, P. R. Levstein, G. Usaj, J. Raya, and J. Hirschinger, Physica A **283**, 166 (2000).
[34] W.H. Zurek, F.M. Cucchietti, and J.P. Paz, Acta Physica Polonica B **38**, 1685 (2007).
[35] C. Petitjean and Ph. Jacquod, Phys. Rev. Lett. **97**, 124103 (2006).
[36] R. Schäfer, T. Gorin, T.H. Seligman, and H.-J. Stöckmann, New J. Phys. **7**, 152 (2005).
[37] S.A. Gardiner, J.I. Cirac, and P. Zoller, Phys. Rev. Lett. **79**, 4790 (1997).
[38] N. Friedman, A. Kaplan, D. Carasso, and N. Davidson, Phys. Rev. Lett. **86**, 1518 (2001); M. F. Andersen, A. Kaplan, and N. Davidson, Phys. Rev. Lett. **90**, 023001 (2003); M. F. Andersen, T. Grünzweig, A. Kaplan, and N. Davidson, Phys. Rev. A **69**, 063413 (2004).
[39] M. F. Andersen, A. Kaplan, T. Grünzweig, and N. Davidson, Phys. Rev. Lett. **97**, 104102 (2006).
[40] N. Chattrapiban, E. A. Rogers, I. V. Arakelyan, R. Roy, and W. T. Hill III, J. Opt. Soc. Am. B **23**, 94 (2006); I. V. Arakelyan, N. Chattrapiban, S. Mitra, and W. T. Hill III, Phys. Rev. A **75**, 061604(R) (2007).
[41] F. Haug, M. Bienert, W.P. Schleich, T.H. Seligman, and M.G. Raizen, Phys. Rev. A **71**, 043803 (2005).
[42] D. Waltner, M. Gutierrez, A. Goussev, and K. Richter, in preparation
[43] M. Sieber and K. Richter, Physica Scripta **T90**, 128 (2001); M. Sieber, J. Phys. A **35**, L613 (2002).